DNA Repair 130 (2023) 103566

Contents lists available at ScienceDirect

DNA Repair

journal homepage: www.elsevier.com/locate/dnarepair

Live cell transcription-coupled nucleotide excision repair dynamics revisited☆

Diana A. Llerena Schiffmacher [a], Katarzyna W. Kliza [b,1], Arjan F. Theil [a], Gert-Jan Kremers [c], Jeroen A.A. Demmers [d], Tomoo Ogi [e,f], Michiel Vermeulen [b,g], Wim Vermeulen [a,*], Alex Pines [a,*]

[a] Department of Molecular Genetics, Erasmus MC Cancer Institute, Erasmus University Medical Center, Dr Molewaterplein 40, Rotterdam 3015 GD, the Netherlands
[b] Department of Molecular Biology, Faculty of Science, Radboud Institute for Molecular Life Sciences (RIMLS), Oncode Institute, Radboud University Nijmegen, Geert Grooteplein Zuid 28, Nijmegen 6525 GA, the Netherlands
[c] Optical Imaging Centre, Erasmus University Medical Center, Dr Molewaterplein 40, Rotterdam 3015 GD, the Netherlands
[d] Proteomics Center, Erasmus University Medical Center, Dr Molewaterplein 40, Rotterdam 3015 GD, the Netherland
[e] Department of Human Genetics and Molecular Biology, Graduate School of Medicine, Nagoya University, Nagoya, Japan
[f] Department of Genetics, Research Institute of Environmental Medicine (RIeM), Nagoya University, Nagoya, Japan, Graduate School of Medicine, Nagoya University, Nagoya, Japan
[g] Division of Molecular Genetics, The Netherlands Cancer Institute, Plesmanlaan 121, Amsterdam 1066 CX, the Netherlands

ARTICLE INFO

Keywords:
TC-NER
DNA repair
CSB
Live cell imaging

ABSTRACT

Transcription–blocking lesions are specifically targeted by transcription-coupled nucleotide excision repair (TC-NER), which prevents DNA damage-induced cellular toxicity and maintains proper transcriptional processes. TC-NER is initiated by the stalling of RNA polymerase II (RNAPII), which triggers the assembly of TC-NER-specific proteins, namely CSB, CSA and UVSSA, which collectively control and drive TC-NER progression. Previous research has revealed molecular functions for these proteins, however, exact mechanisms governing the initiation and regulation of TC-NER, particularly at low UV doses have remained elusive, partly due to technical constraints. In this study, we employ knock-in cell lines designed to target the endogenous CSB gene locus with mClover, a GFP variant. Through live cell imaging, we uncover the intricate molecular dynamics of CSB in response to physiologically relevant UV doses. We showed that the DNA damage-induced association of CSB with chromatin is tightly regulated by the CSA-containing ubiquitin-ligase CRL complex ($CRL4^{CSA}$). Combining the CSB-mClover knock-in cell line with SILAC-based GFP-mediated complex isolation and mass-spectrometry-based proteomics, revealed novel putative CSB interactors as well as discernible variations in complex composition during distinct stages of TC-NER progression. Our work not only provides molecular insight into TC-NER, but also illustrates the versatility of endogenously tagging fluorescent and affinity tags.

1. Introduction

Irradiation, toxic chemicals and endogenously produced metabolites can damage DNA and potentially disturb cell hemostasis. Multiple repair pathways can remove different types of DNA lesions and ensure that crucial cellular processes such as DNA replication and gene transcription can be preserved [1]. A large variety of helix-destabilizing DNA lesions are recognized and removed by nucleotide excision repair (NER), which comprises two distinct sub-pathways, Global Genome (GG)-NER and Transcription-Coupled (TC)-NER. While lesions across the genome are detected and repaired by GG-NER, transcription-blocking lesions (TBLs) require an intricate interplay between the lesion-stalled RNA polymerase II (RNAPII) and TC-NER specific factors, consisting of Cockayne Syndrome protein B (CSB), Cockayne Syndrome protein A (CSA) and UV-stimulated scaffold protein A (UVSSA) [2]. During transcription elongation, RNAPII encounters and stalls at sites of DNA damage, which triggers CSB to bind the DNA at the backside of RNAPII. CSB's translocating activity promotes the forward movement of the transcription machinery over the stalling site [3–6]. However, when bulky lesions are encountered that prevent bypassing of RNAPII, CSB bends the

☆ This Special Issue is edited by Bennett Van Houten.

* Corresponding authors.
E-mail addresses: w.vermeulen@erasmusmc.nl (W. Vermeulen), a.pines@erasmusmc.nl (A. Pines).
[1] Current address: Max Planck Institute of Molecular Physiology, Otto-Hahn-Straße 11, 44227, Dortmund, Germany.

https://doi.org/10.1016/j.dnarep.2023.103566
Received 14 July 2023; Received in revised form 23 August 2023; Accepted 3 September 2023
Available online 9 September 2023

downstream DNA thereby creating a stable CSB-RNAPII interaction [3]. In parallel, CSA is recruited to the damaged DNA site. CSA is a substrate adaptor for Cullin 4-RBX1-DDB1-E3 ubiquitin ligase complexes ($CRL4^{CSA}$) which targets the substrate(s) for ubiquitylation [7,8]. Different factors within the TC-NER process have been proposed to be ubiquitylated by $CRL4^{CSA}$, including CSB [9,10] and RPB1, the largest subunit of RNAPII [8]. Generally, CRLs are activated by a structural change, initiated by the covalent attachment of the ubiquitin-like activator NEDD8 to the Cullin backbone [11]. The ubiquitylation activity of CRLs is kept on leach by the COP9 signalosome, which removes NEDD8 [12]. Additionally, stalled RNAPII-induced ubiquitylation of CSB is counteracted by the recruitment of UVSSA that binds the Ubiquitin carboxyl-terminal hydrolase 7 (USP7), a deubiquitylating enzyme [13–15]. UVSSA's significance extends further by aiding the recruitment of transcription factor TFIIH to the emerging TC-NER complex [14,16,17]. Recently, RNAPII elongation complex structures containing CSB, $CRL4^{CSA}$ and UVSSA were resolved using cryo-electron microscopy (cryo-EM), providing important structural basis for coupling transcription to DNA repair in human cells [10]. The TC-NER process is likely controlled by an intricate dynamic molecular interplay between TC-NER factors and stalled RNAPII, this includes the dynamic ubiquitylation of RNAPII and other TC-NER components, recently identified as key steps in TC-NER in which CSA, UVSSA and CSB are thought to play a prominent role to coordinate repair, fate of lesion-stalled RNAPII, and subsequent transcriptional restart [8,18]. These dynamic interactions, short-lived transactions and TC-NER factor handovers are, however, difficult to capture in these cryo-EM studies and require additional approaches.

While extensive genetic and biochemical research had identified the core NER proteins and defined their biochemical properties, the dynamic assembly and organization of this multi-step repair process remained elusive for several years, until the introduction of green fluorescent protein (GFP) [19]. The ectopic expression of NER factors fused to GFP, in association with live cell imaging experiments, revealed the dynamics of the NER proteins in living cells [20,21]. Most of the dynamic parameters of GFP-tagged NER factors are deduced from fluorescence redistribution after photobleaching (FRAP) assays and experiments using local infliction of DNA damage in living cultured cells [20,21]. In FRAP assays, fluorescent proteins are photobleached in a narrow strip spanning the cell nucleus by a high-intensity laser pulse. The subsequent fluorescence redistribution is monitored in time, providing a measure for the protein's mobility and potential binding to damaged chromatin. To locally inflict DNA damage a UV-C (266 nm) laser device is applied to generate clean NER-specific lesions, allowing the visualization of NER factor recruitment within living cells [22]. GFP-tagging provided tremendous opportunities to gain insight into the molecular mechanism of several GG-NER and core NER proteins [20,23–27]. Although, live cell studies with the TC-NER protein CSB have been performed and provided information on its dynamic association with lesion-stalled RNAPII [5], the majority of live cell imaging studies on TC-NER factors were hampered by the combination of altered physiological protein expression level and small amount of TBLs. Likely, only a minor fraction of TC-NER factors binds to lesion-stalled RNAPII complexes, and this specific interaction remains intricate to discern.

Most intricate cellular processes, including TC-NER, require physiological stoichiometry of molecular machines [10], which may get disturbed by ectopic expression of fluorescently tagged factors. The significance of endogenous expression of GFP-tagged repair factors was already described by the generation of an XPB-YFP knock-in mouse model [28]. XPB is an essential subunit of the transcription initiation and NER factor TFIIH. With the advent of the CRISPR/Cas9 gene-editing technology [29], it has now become possible to incorporate fluorescent proteins into endogenous gene loci in somatic cells, which likely avoids collateral perturbations by overexpression [30–32]. Indeed, the generation of GFP-RPB1 knock-in cells provided an important tool to study the steady-state kinetics of endogenous RNAPII and its degradation after DNA damage [33,34]. Dissecting TC-NER specific dynamic parameters in live cell analyses, however, is complicated by the confounding dynamics of RNAPII at non-damaged genes.

To directly monitor live cell TC-NER kinetics, we generated a CSB knock-in cell line that expresses CSB fused to mClover (CSB-mC KI), a brighter derivate of GFP, from the endogenous *ERCC6/CSB* gene locus. Strikingly, live cell confocal imaging experiments revealed a considerable CSB immobilization to damaged chromatin following irradiation with physiologically low doses of UV-C. With this optimized TC-NER imaging tool, we elucidated new aspects of TC-NER dynamics related to the highly cooperative organization of TC-NER proteins and the role of the dynamic ubiquitylation in regulating the progression of DNA repair. Implementing the results obtained by FRAP, we developed a fluorescence-based single-cell assay that detects in a highly sensitive, quantitative and robust manner whether TC-NER is compromised. In addition, we used this cell line for mass spectrometry (MS)-based proteomics analysis, by employing the mClover tag fused to CSB as an affinity enrichment bait to specifically immuno-precipitate CSB and its interacting proteins. We further discuss the application and potential of this versatile imaging tool to dissect complex biological processes.

2. Material and methods

REAGENT or RESOURCE	SOURCE	IDENTIFIER
Oligonucleotides		
sgCSB exon 21 (5'-AATGTTGTTTAGCAGTATTC-3')	Integrated DNA technologies	N/A
CSB KI forward primer (5'-GTGCACTTTCCATAGAACTTCTGGTGG-3')	Integrated DNA technologies	N/A
CSB KI reverse primer (5'-CAGGTCTTACATTCAGTCAGACCTGTTC-3')	Integrated DNA technologies	N/A
mClover reverse primer (5'-GCCATGTGTAATCCCGGC-3')	Integrated DNA technologies	N/A
sgCSB exon 2	[8]	N/A
sgCSA exon 3 (5'-ATTATCAGCATGTTATCAGG-3')	Integrated DNA technologies	N/A
sgCSA exon 7 (5'-GCCAAGATATAGTCATAACG-3')	Integrated DNA technologies	N/A
CSA KO exon 3 forward primer (5'-AACTTGCCCAGAGCCAAATA-3')	Integrated DNA technologies	N/A
CSA KO exon 3 reverse primer (5'-TTGCTTTGGGGAAGACACAT-3')	Integrated DNA technologies	N/A
CSA KO exon 7 forward primer (5'-CCCCTGTAAACTTCACATTAGC-3')	Integrated DNA technologies	N/A
CSA KO exon 7 reverse primer (5'-GGATGCCCTGTAATCACTGATT-3')	Integrated DNA technologies	N/A
sgXPA exon 1 (5'-GGCGGCTTTAGAGCAACCCG-3')	Integrated DNA technologies	N/A
XPA KO forward primer (5'-CCTTCTCCCGGATGACAAGA-3')	Integrated DNA technologies	N/A
XPA KO reverse primer (5'-CTTCTTCGCTGCACCTCG-3')	Integrated DNA technologies	N/A
sgUVSSA exon 3 (5'-GTCTCACCAGTTCCGGATGC-3')	Integrated DNA technologies	N/A
UVSSA KO forward primer (5'-ATGAAGATGGGAAGGCAGTG-3')	Integrated DNA technologies	N/A
UVSSA KO reverse primer (5'-TCAGCTCCACCCACACATAA-3')	Integrated DNA technologies	N/A
Antibodies		

(*continued on next page*)

(*continued*)

REAGENT or RESOURCE	SOURCE	IDENTIFIER
Donkey-anti-goat CF™ IRDye 770	Sigma-Aldrich	CAT#sab4600375
Goat anti-DDB1	Abcam	ab9194
Goat anti-mouse CF™ IRDye 680	Sigma-Aldrich	CAT#sab4600199
Goat anti-rabbit CF™ IRDye 770	Sigma-Aldrich	CAT#sab4600215
Mouse anti-CSA	Santa Cruz	SC-376981
Mouse anti-Tubulin (B512)	Sigma-Aldrich	CAT#T5168
Rabbit anti- Rpb1 NTD	Cell Signaling Techn	#14958
Rabbit anti-CSA	Abcam	ab240096
Rabbit anti-CSA	Abcam	ab137033
Rabbit anti-CSB	antibodies-online.com	ABIN2855858
Rabbit anti-DDB1	Novus biologicals	NBP2–75465
Rabbit anti-H2B	Merk Millipore	07–371
Rabbit anti-XPA	Genetex	CAT#GTX103168
Rabbit anti-XPB	Santa Cruz	CAT#sc-293
Bacterial strains		
One Shot™ Top10 Chemically competent cells	Invitrogen	CAT#C4040–06
Chemicals		
[$^{12}C_6$,$^{14}N_4$]-arginine	Silantes	CAT#201003902
[$^{12}C_6$]-lysine	Silantes	CAT#211004102
[$^{13}C_6$,$^{15}N_4$]-arginine	Cambridge Isotope Laboratories	CAT#CNLM-539-H-1
[$^{13}C_6$]-lysine	Cambridge Isotope Laboratories	CAT#CNLM-291-H-1
2 × Laemmli sample buffer	Sigma-Aldrich	CAT#S3401
4′,6-diamidino-2-phenylindole (DAPI)	Sigma-Aldrich	CAT#D9542
5-Ethynyl-uridine (5-EU)	Axxora	JBS-CLK-N002
Acetic acid	Sigma-Aldrich	33209-M
Aqua-Poly/Mount	Polysciences, Inc.	CAT#18606–20
Ascorbic Acid	Sigma-Aldrich	CAT#209198
Atto 594 Azide	Atto Tec	CAT#AD594–105
Benzonase® Nuclease	Novagen/Millipore	CAT#70664
Bovine Serum Albumin (BSA)	Sigma-Aldrich	A3294
Briljant Blue R	Sigma-Aldrich	B-0149
$CuSO_4 * 5 H_2O$	Sigma-Aldrich	CAT#A0278
Dialyzed fetal calf serum	Gibco	CAT#26400044
DMEM for SILAC	ThermoScientific	15786803
DMEM, high glucose, HEPES, no phenol red	Gibco™	21063045
Dulbecco's modified Eagle's medium (DMEM)	Gibco™	11965084
EDTA-free Protease Inhibitor Cocktail	Roche	11836170001
Fetal calf serum (FCS)	Capricorn	FBS-12A
Flavopiridol hydrochloride hydrate	Sigma-Aldrich	F3055
Formaldehyde solution	Sigma-Aldrich	47608
HEPES	Gibco™	15630080
Hoechst 34580	Life Technologies	H21486
JetPEI Transfection reagent	Polyplus	101–10 N
L-Proline	Sigma-Aldrich	P0380–100 G
Magnesium chloride ($MgCl_2$)	Fluka	63072
Methanol	Honeywell	32213
MG132	Enzo	BML-PI102
MLN4924 (NAE1i)	Boston Biochem	I-502
Nonidet P 40 Substitute (NP40)	Fluka	74385
Sodium chloride (NaCl)	Sigma-Aldrich	71380-M
Penicillin/streptomycin (PS)	Sigma-Aldrich	P0781
Puromycin	InvivoGen	CAT#ant-pr-1
PVDF Membrane	Merk Millipore	IPVH00010
Sodium dodecyl sulfate (SDS)	Sigma-Aldrich	71729
Spironolactone	Sigma-Aldrich	CAT#S3378
Sucrose	Sigma-Aldrich	84100
THZ1	Xcessbio.com	M60214–2S
Triton™ X-100	Sigma-Aldrich	T8787
Trizma® base	Sigma-Aldrich	T6066
TWEEN® 20	Sigma-Aldrich	P1379
Commercial kits		
4D-Nucleofector™ X Kit	Lonza	V4XC-1024
PureLink® Genomic DNA Mini Kit	Invitrogen	K182001
Experimental models: cell lines		
HCT116 Wild type	[8]	N/A
HCT116 CSB KO	This paper	N/A
HCT116 CSB-mClover (clone #1)	This paper	N/A
HCT116 CSB-mClover (clone #2)	This paper	N/A
HCT116 CSB-mClover CSA KO (clone #1)	This paper	N/A
HCT116 CSB-mClover CSA KO (clone #2)	This paper	N/A
HCT116 CSB-mClover XPA KO (clone #1)	This paper	N/A
HCT116 CSB-mClover XPA KO (clone #2)	This paper	N/A
HCT116 CSB-mClover UVSSA KO	This paper	N/A
U2OS CSB-mClover	This paper	N/A
U2OS CSB-mClover CSA KO	This paper	N/A
U2OS CSB-mClover UVSSA KO	This paper	N/A

(*continued on next page*)

(*continued*)

REAGENT or RESOURCE	SOURCE	IDENTIFIER
Recombinant DNA		
Lenti-CRISPRv2	Addgene	CAT#52961
Software and algorithms		
Fiji ImageJ	https://imagej.net/Fiji	N/A
LAS AF (version 3.3.0.16799)	Leica Microsystems	N/A
MaxQuant software suite (1.6.3.3)	[35]	N/A
Opera Phenix	PerkinElmer	N/A
Perseus (version 1.6.14.0)	[36]	N/A
Prism GraphPad (version 8.2.1)	GraphPad software Inc.	N/A
Tracking of Indels by DEcomposition (TIDE)	http://shinyapps.datacurators.nl/tide/	N/A
Other		
4D-Nucleofector® Core and X unit	Lonza	AAF-1003B and AAF-1003X
Bioruptor Sonication System	Diagenode	N/A
GelCount	Oxford Optronix	N/A
GFP-Trap-A® agarose bead slurry	ChromoTek	CAT#gta-100
Mass spectrometer Orbitrap Lumos™ Tribrid™	ThermoScientific	N/A
Mini-PROTEAN TGX™ Precast Protein Gels	BioRad	CAT#456–1084
NuPAGE™ 4–12 % Precast Protein Gels	Invitrogen	NP0321BOX
NuPAGE™ MOPS SDS running buffer	Invitrogen	NP0001
Odyssey® Imaging System	LI-COR	N/A
SensoPlate™, 96 well, glass bottom	Greiner	655892
TUV lamp (UV-C)	Phillips	N/A

2.1. Generation of CSB-mClover knock-in cell lines and culture conditions

HCT116 colon cancer or U2OS osteosarcoma cells were co-transfected with LentiCRISPR-V2 puro plasmid encoding a sgRNA targeting the last protein-coding base pairs in exon 21 of *ERCC6/CSB* and with a designed donor plasmid containing two 300 bp homology regions enclosing the cut site, introducing a 15 amino acid linker, two TEV cleaving sites [37] and mClover3 [38] (gene synthesis services GenScript, sequence upon request, Fig. 1A and Supplementary Fig1 A). Cells were co-transfected following either the jetPEI protocol (for HCT116) or the SE Cell Line 4D-Nucleofector™ X Kit protocol (for U2OS), according to manufacturer instructions. Two days post-transfection, cells were either selected with 2 ug/ml puromycin or sorted for mClover-positive cells by FACS. Single clones were isolated and screened by immunoblotting, PCR and sequencing. For PCR, genomic DNA was isolated using PureLink® Genomic DNA Mini Kit and primer combinations for which the amplicon changes in size upon integration of mClover and which were tag specific. Cells were either cultured in Dulbecco's modified Eagle's medium (DMEM) or in phenol red-free DMEM for live imaging experiment, supplemented with 10 % fetal calf serum, 1 % penicillin/streptomycin. The cells were kept in a humidified incubator at 37 °C and 5 % CO_2.

2.2. Generation of knockout cells

For generating the CSA, XPA or UVSSA knockouts (KO's) and the CSB-mClover knock-ins (HCT116: CSB-mC KI; U2OS: CSB KI) cells were transfected with a LentiCRISPR-V2 puro plasmid containing specific sgRNAs, using the jetPEI protocol and puromycin selection as described above. While *ERCC8*/CSA was targeted by two sgRNAs in exon 3 and exon 7, XPA and UVSSA were targeted by a single sgRNA, cutting either in the first or third exon of the gene, respectively. Single clones were expanded and KO's were verified by immunoblotting. For PCR, genomic DNA was isolated as previously described and for each exon a specific primer combination was used. The amplicon was sequenced and insertion/deletion (indel) frequency was analyzed by Tracking of Indels by DEcomposition (TIDE) using the TIDE web tool.

2.3. UV-C survival assay

1000 cells were seeded in 10 cm dishes in duplicate, or 750 cells were seeded in 6-well in triplicate, and were either mock or UV-C-irradiated with 4, 8 or 12 $J.m^{-2}$ 24 h after seeding (254 nm). 7–10 days post-UV, cells were fixed and stained with 50 % methanol, 10 % acetic acid, and 0.1 % Brilliant Blue R. After colony counting using GelCount, each cell line was normalized to the mock-treated condition, which was set to 100 % survival.

2.4. RNA synthesis recovery assay

250.000 cells were seeded on glass coverslips two days prior to UV-C (10 $J.m^{-2}$) treatment. 24 h post-UV, nascent RNA was labeled with 0.2 mM 5-Ethynyl-uridine (5-EU) in culture medium for 1 h. Cells were fixed with 4 % formaldehyde in PBS, permeabilized with 0.1 % Triton X-100 in PBS and blocked with 1.5 % BSA in PBS at room temperature (RT). Next, ATTO 594 Azide was coupled to 5-EU by Click-it®. In short, cells were incubated with Click-it® solution (50 mM Tris-HCl pH 7.6; 60 µM ATTO 594 Azide; 4 mM CuSO4 *5H2O; 10 mM Ascorbic Acid) for 1 h in the dark at RT, washed 3 times with 0.1 % Triton X-100 in PBS, followed by two PBS washes and DAPI staining. Coverslips were mounted using Aqua-Poly/Mount and cells were imaged using an LSM700 microscope equipped with a 40x Plan-apochromat 1.3 NA oil immersion lens (Carl Zeiss). Nuclear DAPI and ATTO 594 intensities were determined using Fiji and an ImageJ macro.

2.5. Whole-cell extract

Cell pellets were lysed in denaturing lysis buffer (2 % SDS, 1 % NP-40, 150 mM NaCl, 50 mM Tris pH 7.5) with additional 50 U Benzonase® nuclease for 10 min at RT in rotation. Lysates were centrifuged at maximum speed for 10 min and equal volumes of supernatant and 2x Laemmli-SDS sample buffer were heated at 98 °C for 5 min

2.6. Fractionation

Cells were either mock or UV-C irradiated (30 $J.m^{-2}$), collected at the indicated time points and lysed in cold IP buffer (30 mM HEPES pH 7.5; 130 mM NaCl; 1 mM $MgCl_2$; 0.5 % Triton X-100; 1x EDTA-free Protease Inhibitor Cocktail) for 10 min on ice. Lysates were cleared by centrifugation at 21000xg 10 min at 4 °C, separating the supernatant (soluble fraction) from the cell pellet (chromatin-containing fraction), which was lysed using the denaturing lysis buffer, described in Section 2.5. Equal volumes of 2x Laemmli-SDS sample buffer were added to both fractions in a 1:1 ratio and samples were heated at 98 °C for 5 min, followed by

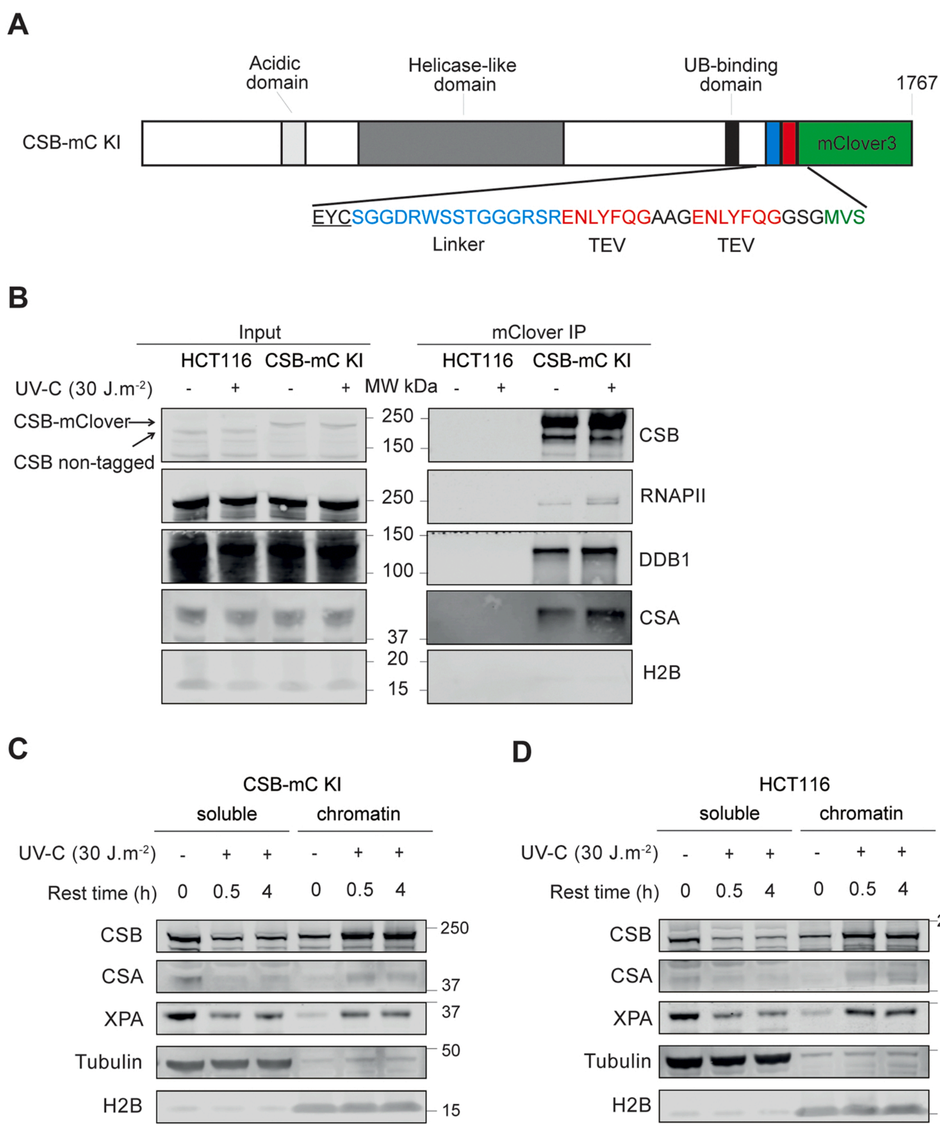

Fig. 1. Generation and validation of CSB-mC KI cells. (A) Schematic representation of the resulting fusion protein CSB-mClover: grey/black boxes represent important functional domains in CSB; blue box is the linker amino acid sequence between CSB and the added tags; red box are the two TEV protease recognition sequences; green, represents the mClover coding sequence. (B) Immunoprecipitation of CSB-mClover from whole cell protein extracts of HCT116 or CSB-mC KI, either mock treated or collected 30 min after 30 J.m^{-2} UV-C irradiation, followed by immunoblot analysis of the indicated proteins. (C-D) Immunoblotting of CSB, CSA and XPA in soluble and chromatin fractions, in response to UV-C irradiation from (C) CSB-mC KI and (D) HCT116 cells. Cells were mock treated or exposed to 30 J.m^{-2} of UV-C and collected after the indicated time points. Tubulin and H2B antibodies were used as markers for the soluble and chromatin fraction, respectively.

SDS-PAGE separation as described in Section 2.7.

2.7. Immunoprecipitation and immunoblotting

Cells were either mock or irradiated with 30 J.m^{-2} of UV-C and lysed after 30 min in cold IP buffer (30 mM HEPES pH 7.5; 130 mM NaCl; 1 mM $MgCl_2$; 0.5 % Triton X-100; 1x EDTA-free Protease Inhibitor Cocktail) for 10 min on ice. After 10 cycles of sonication using the Bioruptor Sonicator (15 s on; 45 s off) at 4 °C, cold IP buffer supplemented with 500 U Benzonase® nuclease was added and samples were kept in rotation for 1–2 h at 4 °C. Following a centrifugation step at 21000xg for 10 min at 4 °C, the supernatants were collected and are here after called whole-cell extract.

CSB-mClover complexes were pulled down from whole-cell extracts during a 1 h incubation with GFP-Trap®A beads, in rotation at 4 °C. The beads were subsequently washed 3 times with cold IP buffer and isolated by centrifugation at 700xg. For immunoblotting, proteins were denatured by boiling the beads in 2x Laemmli-SDS sample buffer at 98 °C for 5 min

Proteins were separated by SDS-PAGE using either 4–12 % Bis-Tris NuPAGE® gels with MOPS running buffer, Mini-PROTEAN TGX™ gels or hand casted 6 % acrylamide gels with a Tris-Glycine-SDS buffer. Separated proteins were transferred onto PVDF membranes (0.45 µm) overnight at 4 °C, which were blocked in 5 % BSA in PBS and probed with the appropriate primary antibodies (resources table). Next, membranes were washed with PBS containing 0.05 % Tween-20 and incubated with IRDye-conjugated secondary antibodies (resources table). Proteins were visualized by the Odyssey® Imaging System.

2.8. Fluorescence recovery after photobleaching

Fluorescence recovery/redistribution after photobleaching (FRAP) experiments were performed as described previously [33,34] using an Leica SP5 or SP8 confocal laser-scanning microscope with a 40 × /1.25 NA HC PL APO oil immersion lens, in a controlled environment at 37 °C and 5 % CO_2. HCT116 CSB-mC KI or U2OS CSB-mC KI cells, as well as the generated CSA KO, XPA KO or UVSSA KO cells, were seeded on glass coverslip two days prior to live imaging experiments and were treated with indicated UV-C doses and/or incubated with transcription inhibitors THZ1 (1 µM) or Flavopiridol (1 µM) or with TFIIH inhibitor spironolactone (10 µM) 1 h prior to UV-C irradiation or with CRL inhibitor MLN4924 (NAE1i) (10 µM) 30 min before UV-C treatment and imaging (resources table). Cells were maintained with inhibitors during imaging. To measure CSB-mClover mobility, GFP fluorescence was first monitored every 200 ms at 400 Hz with a zoom of 8x in a strip of 512 × 16 pixels across the nucleus until reaching steady state of the signal (pre-bleach), then photobleached at maximum laser intensity, and lastly, fluorescence recovery was followed every 200 ms using low laser intensity (post-bleach). Fluorescence intensity was background-corrected, normalized to the average of the last 30 pre-bleach frames and set to 100 %. During one experiment for each condition at least 10 cells were measured. The immobile fraction (F_{imm}) represents the ratio between the post-bleach fluorescence intensity of mock and either inhibitor-treated, UV-C-irradiated or KO cells. F_{imm} was calculated as described in [26] with the formula: $F_{imm} = 1 - (I_{final,\ treat} - I_{0,\ treat})/(I_{final,\ untr} - I_{0,\ treat})$.

2.9. Fluorescence-based single-cell assay

8000 U2OS wild type (hereafter called U2OS), CSB KI cells, as well as the corresponding CSA KO or UVSSA KO cells were seeded in triplicate in a 96 well SensoPlate™ suited for fluorescent imaging two days prior to UV-C (6 $J.m^{-2}$). Cells were allowed to recover from irradiation either 1 or 7 h. Each well was washed with PBS, followed by pre-extraction with room temperature CSK buffer (20 mM HEPES pH 7.6; 0.5 % Triton X-100; 50 mM NaCl; 3 mM $MgCl_2$; 300 mM sucrose) for 3 min, fixation with 4 % formaldehyde in PBS for 5 min and two PBS washes. Next, the cells were treated with 0.1 % Triton X-100 in PBS for 5 min and washed 3 times with PBS within 10 min. Cells were kept in PBS with Hoechst, protected from light at 4 °C, and imaged within 1 week using the automated spinning disk confocal HCS system (Opera) equipped with a 40 × 1.1 NA Plan Apochromat water immersion objective and two sCMOS cameras (0.3 μm ×0.3 μm pixel size). Nuclei were identified by Hoechst staining, followed by the quantification of the mClover signal, which was background-corrected via U2OS cells and normalized to the non-irradiated CSB-mClover condition (set to 1).

2.10. SILAC labelling, chromatin fraction and mass spectrometry

For mass spectrometry experiments, proteins were labeled with stable isotope labeling of amino acids in culture (SILAC) for at least 5 passages. Cells were cultured in DMEM for SILAC supplemented with 10 % dialyzed FBS, 1 % penicillin/streptomycin and 0.2 mg/ml L-Proline. In addition, either unlabeled L-arginine-HCl and L-lysine-HCL (Light medium) or $^{13}C_6,^{15}N_4$ L-arginine-HCl and $^{13}C_6,^{15}N_2$ L-lysine-2HCL (Heavy medium) was added.

Equal number of cells were either mock or UV-C irradiated (30 $J.m^{-2}$) and collected after 30 min. Cell pellets were lysed in cold IP buffer (30 mM HEPES pH 7.5; 130 mM NaCl; 1 mM $MgCl_2$; 0.5 % Triton X-100; 1x EDTA-free Protease Inhibitor Cocktail) for 10 min on ice. Lysates were cleared by centrifugation at maximum speed for 10 min at 4 °C. The obtained cell pellets were lysed in cold IP buffer a second time for 10 min on ice. Next, DNA was fragmented by sonication (15 s on; 45 s off) using the Bioruptor Sonicator at 4 °C, followed by the addition of cold IP buffer supplemented with 500 U Benzonase® nuclease. The samples were kept in rotation for 1 h at 4 °C and cleared by centrifugation at 21000xg for 10 min at 4 °C. The supernatants were collected and are hereafter referred to as chromatin fraction.

CSB-mClover protein complexes were pulled down from chromatin-enriched protein extracts with GFP-Trap®A beads as described previously [39]. Eluted proteins in Laemmli-SDS sample buffer were separated on 4–12 % Bis-Tris NuPAGE® gels with MOPS running buffer and visualized with Coomassie staining. After cutting the gel lanes into 2-mm slices, the proteins were in-gel reduced with dithiothreitol, alkylated with iodoacetamide and digested with trypsin. Nanoflow liquid chromatography tandem mass spectrometry (LC-MS/MS) was performed with an EASY-nLC™ 1200 capillary liquid chromatography system connected to an Orbitrap Lumos™ Tribrid™ mass spectrometer operating in positive mode. Peptide samples were retained on a ReproSil C18 reversed phase column (1.5 cm × 100 μm) with a flow rate of 8 μL/min. Separation was achieved by gradually increasing the amount of acetonitrile (in 0.1 % formic acid) from 0 % to 80 % over a period of 60 min and a flow rate of 200 nL/min using a splitter, and samples were sprayed into the electrospray ionization (ESI) source of the machine. Mass spectra were collected in continuum mode, and peptide fragmentation was performed in data-dependent mode. Raw data analysis was conducted using MaxQuant software (1.6.3.3) and further analysis was performed using Perseus (1.6.14.0).

2.11. Statistical analysis

Mean values, as well as each individual value and S.D. (in red) or S.E. M. (in black) error bars are shown for each experiment. Multiple *t*-tests (unpaired, two-tailed) were used to determine statistical significance between groups, followed by multiple comparison correction with the Holm-Sidak method without assuming a consistent standard deviation. For the analysis of Supplementary Fig. 2D and E, a nested *t*-test was performed with significance levels set to 0.05. For the statistical significance analysis of IF data, we applied a nested One-Way ANOVA using the Brown-Forsythe and Welch ANOVA tests, followed by post-hoc analysis with the Games-Howel method. All analyses were performed using Graph Pad Prism version 8.2.1 for Windows (GraphPad Software, La Jolla California USA). P values expressed as $*P < 0.05$; $**P < 0.01$, $***P < 0.001$, $****P < 0.0001$ were considered to be significant, otherwise as non-significant (n.s.).

3. Results

3.1. Generation and validation of endogenously tagged CSB

With the emergence of CRISPR-Cas9 mediated genome editing, we were able to generate homozygous knock-in cell lines that express a fluorescently tagged version of CSB under its endogenous promoter. The DNA sequence of the mClover was inserted at the 3' end of the CSB gene and sequence verified (Fig. 1A; Supplementary Fig. 1A). The expression of CSB-mClover remains under the control of its native promoter, resulting in a physiologically relevant expression of the fusion protein (CSB-mClover) that closely mirrors that of non-tagged CSB in wild type cells (HCT116) (Fig. 1B; Supplementary Fig. 1B). To investigate whether mClover interferes with CSB function in TC-NER, we irradiated the cells with UV-C and performed colony survival and recovery of RNA synthesis (RRS) assays after UV-irradiation. Two independent CSB-mClover knock-in clones (hereafter, CSB-mC KI and CSB-mC KI #2) were similarly UV-resistant as the parental cell line expressing endogenous non-tagged CSB, in contrast to CSB KO cells that were highly UV-sensitive (Supplementary Fig. 2A-C). Additionally, CSB-mC KI cells equally recovered RNA synthesis 24 h after UV-irradiation as parental HCT116 cells, while CSB KO cells were unable to resume RNA synthesis (Supplementary Fig. 2D-E). To further validate the CSB-mC KI cells, we examined the subcellular distribution of CSB in UV-C-irradiated cells after cell lysate fractionation and its complex composition by immunoprecipitation (IP) using GFP-Trap beads. Immunoblot analysis showed that CSB-mClover mainly relocated to the chromatin-containing fraction after UV-C irradiation similar as non-tagged CSB (Fig. 1C-D). Moreover, CSB-mClover IP confirmed the previously found association with RNAPII and with the $CRL4^{CSA}$ complex (CSA and DDB1) (Fig. 1B). Together, these data showed that the endogenously expressed mClover-tagged CSB remains fully functional in TC-NER and thus validate the CSB-mC KI cell line as a *bona fide* tool for further analysis.

3.2. CSB knock-in cells enable in-vivo imaging of TC-NER reaction at a physiological UV dose

Previous results, using stably overexpressing GFP-CSB, indicated that CSB dynamically associates with the transcription machinery [5] and that after a relatively high dose of UV-C (16 $J.m^{-2}$) only a minor fraction of CSB becames immobilized in a transcription-dependent manner. 16 h after UV treatment, when the majority of UV lesions were repaired and transcription had fully recovered, GFP-CSB mobility reverted to the undamaged situation, suggesting that GFP-CSB immobilization reflects its binding to UV-damaged chromatin and its involvement in TC-NER. However, this limited dynamic window of GFP-CSBs mobility in response to TC-NER induction hampered further in-depth mechanistic analysis. Given that non-physiological CSB expression may affect the FRAP assay, we speculated that endogenously expressed of CSB-mClover would be more suitable for this analysis. In agreement with this hypothesis, FRAP experiments conducted in CSB-mC KI cells demonstrated that the majority of CSB became chromatin bound after 8 J.m^{-2} UV-C irradiation, whereas the same live cell imaging conditions applied to GFP-CSB-overexpressing cells did not yield the same chromatin binding outcome (Supplementary Fig. 3A).

FRAP experiments showed a marked CSB immobilization of ~40 % at physiologically relevant low dose of 4 J.m^{-2} UV-C. Importantly, this immobilization was reversible, as CSB mobility partially recovered 4 h after UV-C irradiation and fully returned to normal after 16 h (Fig. 2A). Moreover, the extent of immobilization appeared to be UV dose-dependent, with a larger fraction of about 60 % of the total CSB

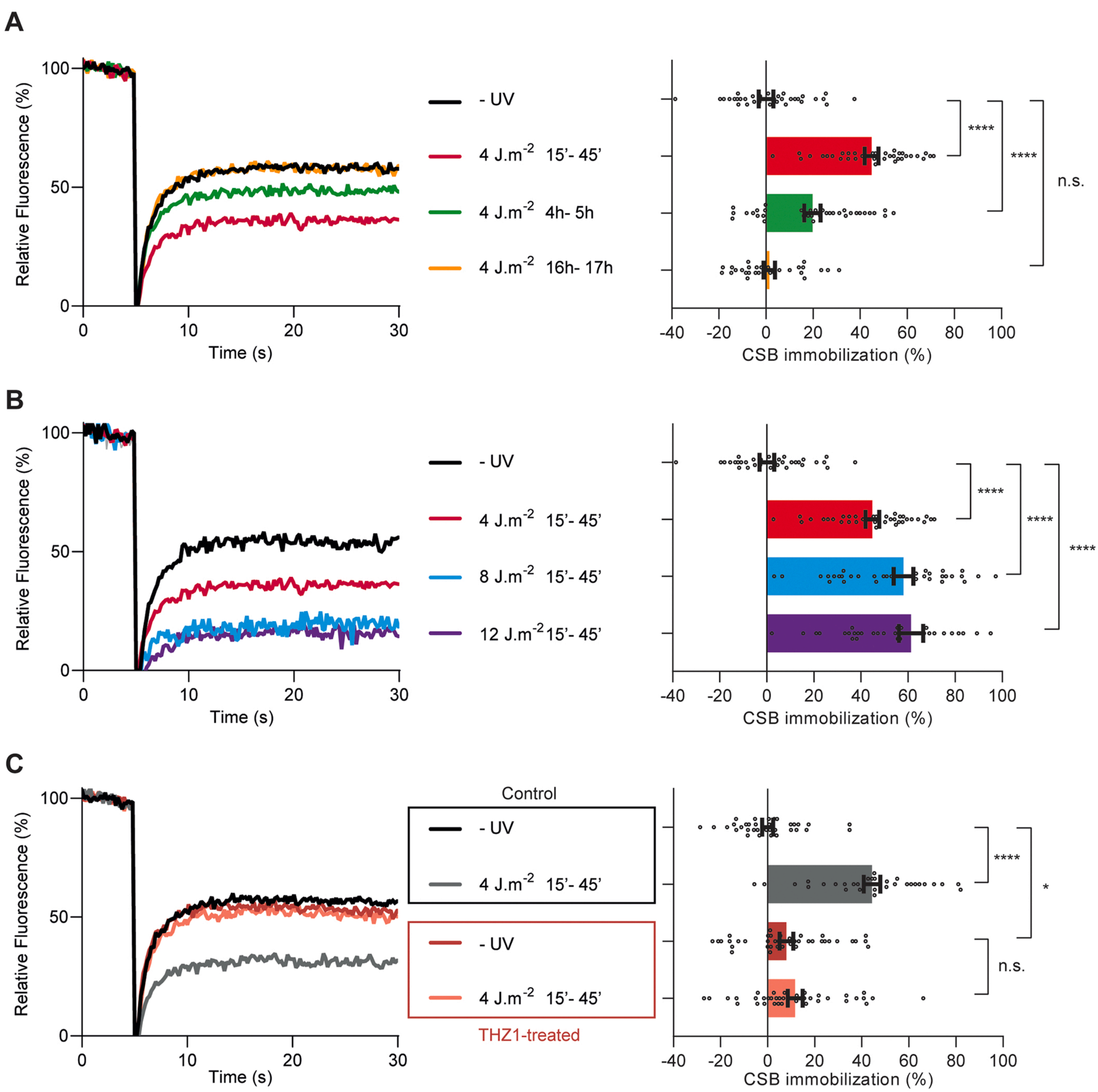

Fig. 2. Transcription- and dose-dependent CSB immobilization to UV-C-induced TBLs determined by Fluorescence Recovery After Photobleaching (FRAP) analysis. (A-C) Left panels: Fluorescence redistribution curves of CSB-mC KI cells (A) mock or UV-C irradiated with 4 J.m^{-2}; (B) mock or UV-C irradiated with 4, 8, or 12 J.m^{-2}; (C) mock or UV-C irradiated with 4 J.m^{-2} in presence or absence of THZ1. Fluorescence redistributions were measured at the indicated time points. Fluorescence redistribution was measured during 30 s after bleaching and normalized to average pre-bleach intensities (100 %). Right panels: Percentage of CSB-mClover immobile fraction in CSB-mC KI cells calculated from FRAP analyses shown in the left panel, see methods. Graphs and FRAP curves depict the mean & S.E.M. of ≥ 30 cells from at least three independent experiments. * * $P < 0.01$, * ** $P < 0.001$, * ** * $P < 0.0001$, n.s. non-significant, analyzed by unpaired, two-tailed *t*-test (adjusted for multiple comparisons, see "Methods").

protein pool becoming immobilized which reached saturation around this dose (Fig. 2B). To prevent RNAPII from encountering TBLs, CSB-mC KI cells were incubated with the transcription inhibitors, THZ1 and Flavopiridol, which respectively inhibit CDK7 and CDK9. FRAP analysis on cells treated with these transcription inhibitors prior to UV-irradiation resulted in the absence of CSB immobilization, confirming that CSB binding is transcription-dependent (Fig. 2C; Supplementary Fig. 3B). To assess whether this phenotype was not a clonal peculiarity, the results were confirmed in a second independent CSB-mC KI clone (Supplementary Fig. 3C). Previous studies[9] have shown that CSB gets degraded after higher doses of UV. To examine whether the observed apparent CSB-mClover immobilization is not influenced by its degradation, we determined the protein levels in cells irradiated with 4, 8 and 12 J.m^{-2} of UV-C by immunoblotting (Supplementary Fig. 3D) and measured the fluorescent intensity of CSB-mClover during FRAP experiments at 4 J.m^{-2} (Supplementary Fig. 4A). Indeed, under those conditions we observed some reduction in CSB protein levels, although only to a minor extent. These results are in line with other previous studies, observing marginal CSB degradation following UV-C irradiation [40,41]. Importantly, these observations suggest that the observed UV-induced CSB immobilization, as deduced from the incomplete fluorescence recovery in the FRAP analysis, is not strongly affected by fluorescence loss due to CSB-mClover degradation.

Our findings suggest that fluorescently tagged CSB, expressed from the endogenous promoter is a powerful and unprecedented highly sensitive tool for studying the TC-NER process at physiological UV doses by live cell imaging.

3.3. CRL4^{CSA} ubiquitin ligase activity affects CSB mobility

Although the protein function of CSB [3] has been characterized and structural insight has been obtained how CSB and CRL4^{CSA} bind to RNAPII [10], it remains unknown how CSB is controlled and interconnected in vivo with CSA. CSA is a component of the CRL4^{CSA} complex and coordinates the successive molecular interactions during TC-NER by ubiquitylation. To uncover the importance of CRL4^{CSA} ubiquitylation activity on CSB dynamics during TC-NER, we made use of the specific inhibitor MLN4924 (NAE1i). MLN4924 inhibits the neddylation of Culin4, which is required for the activation of the CRL4^{CSA} complex [42]. FRAP experiments revealed no difference in CSB mobility between mock and cells treated with NAEi (0.5 and 4.5 h) in absence of DNA damage as well as within 1 h after UV irradiation (4 J.m^{-2}, Fig. 3A, Supplementary Fig. 4B). However, while the control cells showed resumption of mobility 4 h after UV irradiation, no recovery and even more immobilization of CSB was detected in presence of NAE1i (Fig. 3A). These data indicate that CSB remains bound to UV-damaged chromatin and that the release, rather than the recruitment of CSB is affected by inhibiting neddylation and subsequent ubiquitylation.

We questioned if CRL4^{CSA} is the main ubiquitin ligases responsible for CSB dissociation since NAE1i may act on multiple CRL complexes. To this end, we knocked out CSA by CRISPR/Cas9-editing in the CSB-mC KI cell line (Supplementary Fig. 1C) and validated TC-NER parameters. As expected, CSA knockout (KO) cells were unable to resume RNA synthesis and showed strong UV sensitivity (Supplementary Fig. 2B-C,E). Furthermore, the CSB-mClover protein levels in CSA KO were similar to the parental wild-type (WT) cell line (Supplementary Fig. 4A,C), and the loss of CSA did not affect CSB ability to translocate to the chromatin-containing fraction after UV-C irradiation (Supplementary Fig. 4D). FRAP analysis revealed that UV-induced CSB immobilization was equally affected in CSA KO as in WT cells treated with NAE1i (Fig. 3B; Supplementary Fig. 4E). Additionally, we did not observe any additive effect on CSB mobility by FRAP in CSA KO cells treated with NAE1i, suggesting CRL4^{CSA} is the main player coordinating CSB recycling (Supplementary Fig. 4F). Further investigation is needed to determine whether the release of CSB from lesion-stalled RNAPII is a direct consequence of CRL4^{CSA}-mediated CSB ubiquitylation [9,10], an indirect effect of ubiquitylating other TC-NER targets, such as RPB1 [8], or simply due to the TC-NER progression being halted in the absence of CSA.

3.4. CSB degradation upon loss of UVSSA

To investigate whether absence of further downstream TC-NER factor UVSSA has a similar effect on CSB dissociation as absence of CSA [17], we generated UVSSA KO in CSB-mC KI cell line. The homozygous deletion was validated through sequencing, and TC-NER deficiency was confirmed by UV survival (Supplementary Fig. 5A-B). UVSSA is essential for TC-NER as it protects CSB from UV-induced degradation by recruiting the de-ubiquitylating enzyme USP7 and facilitates the loading of the downstream TFIIH complex. In the absence of UV-induced DNA damage, the lack of UVSSA had no impact on the mobility of CSB. Surprisingly, in response to 4 J.m^{-2} UV-C, we noticed an even stronger CSB immobilization in UVSSA KO as compared to WT cells, when measured within the first hour after irradiation (Supplementary Fig. 5C). However, at later time points post UV, the FRAP assay could not be performed due to the virtual complete degradation of CSB in UVSSA KO cells, which occurred already within the first 2 h after UV-treatment in UVSSA KO cells (Supplementary Fig. 5D). These data further confirm that UVSSA is indeed needed for the stabilization of CSB during active TC-NER [13–15]. The protein level of CSB was rescued by the treatment of NAE1i before UV-irradiation in UVSSA KO cells (Supplementary Fig. 5E), suggesting a direct role of CRL4^{CSA} in the degradation process of CSB. However, in line with the previous FRAP experiments, NAE1i prevented the resumption of the mobility of CSB (Fig. 4A) and could thus not be used to study the TC-NER dynamics in the absence of UVSSA. The data on chromatin-binding and protein breakdown of CSB were confirmed by immunoblot analysis. CSB translocated rapidly from the soluble fraction to the chromatin upon UV-C irradiation (30 J.m^{-2}) and, in absence of UVSSA, CSB protein degradation was evident after 4 h and rescued by NAEi (Supplementary Fig. 5F). Together the data suggest that the mobility and degradation of CSB are coordinated by both UVSSA- and CSA-containing complexes, in which ubiquitylation plays a crucial role.

3.5. TC-NER progression affects molecular dynamic of CSB

To explore whether persistent binding of CSB to TBL-stalled RNAPII is a direct consequence of the absence of CRL4^{CSA}-mediated ubiquitylation or results from a TC-NER progression defect, we knocked out XPA (XPA KO) in the CSB-mC KI cell line (Supplementary Fig. 1D). XPA is essential for both GG-NER and TC-NER by assisting TFIIH in damage verification and its key role in the assembly and stabilization of the pre-incision complex [2,43]. Cells that lack XPA are unable to excise the damaged strand and as a consequence do not complete the NER pathway. Two independent XPA KO clones were validated by colony survival and RRS analysis (Supplementary Fig. 2B-C,E). Moreover, XPA KO did not affect ability of CSB and CSA to translocate to the chromatin-containing fraction after UV-C irradiation (Supplementary Fig. 6A). FRAP analysis revealed that neither the CSB mobility in non-irradiated cells nor CSB immobilization 1 h after 4 J.m^{-2} was affected by the loss of XPA. However, CSB remained immobilized 4 h post UV (Fig. 4B, Supplementary Fig. 6B). Similar to what was found in WT cells, only a small reduction on CSB protein levels in XPA KO cells was observed after UV damage by fluorescent intensity analysis (Supplementary Fig. 6C), suggesting that the observed CSB mobility is not dependent on its degradation.

Since XPA interacts and cooperates with the multi-protein complex TFIIH during damage verification in NER, we investigated whether the loss of TFIIH would induce a similar phenotype on CSB mobility as loss of XPA. To address this, we treated CSB-mC KI cells with spironolactone, a mineralocorticoid and androgen receptor antagonist found to degrade XPB [44,45]. While spironolactone-treated cells showed no aberrant

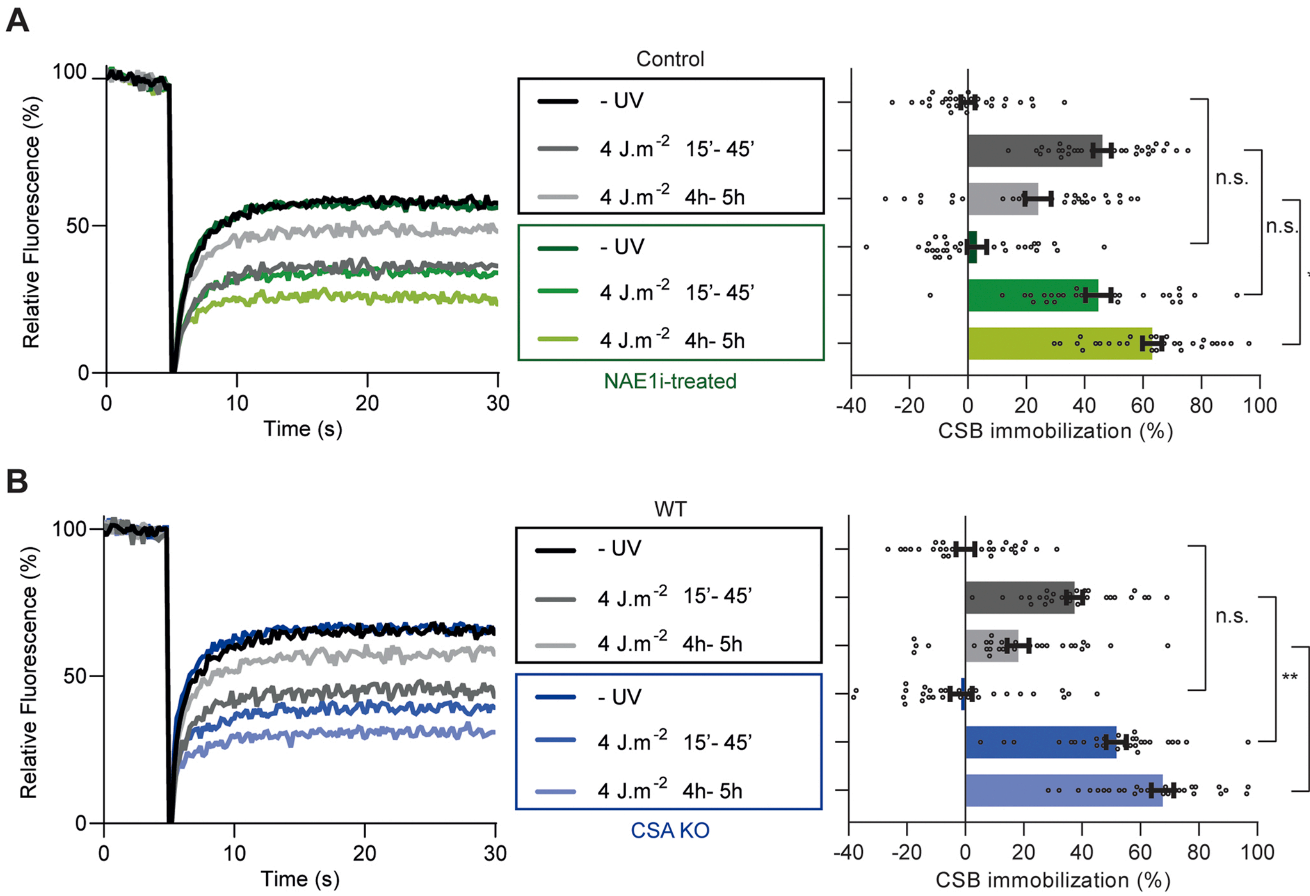

Fig. 3. TBL release of CSB is CRL4^{CSA}-dependent. (A-B) Left panels: FRAP analysis of CSB-mC KI cells. (A) WT KI cells mock (grey shades) or 10 μM NAE1i-treated (green shades). (B) Comparison of WT (grey shades) and CSA KO (blue shades). Cells were either mock or UV-C-irradiated (4 J.m^{-2}) and measured at the indicated time points. Fluorescence recovery was measured and normalized as described in Fig. 2. Right panels: Percentage of CSB-mClover immobile fraction in CSB-mC KI cells calculated from FRAP analysis shown in the left panel, as described in Fig. 2. Graphs and FRAP curves depict the mean ± S.E.M. of 30 cells from three independent experiments. * * $P < 0.01$, * ** $P < 0.001$, * ** * $P < 0.0001$, n.s. non-significant, analyzed by unpaired, two-tailed *t*-test.

behavior in the non-irradiated or 1 h after UV irradiation, release of CSB 4 h after UV irradiation was strongly impaired, indicating that TFIIH as well as XPA are essential for the proper release of CSB from TBLs (Fig. 4C).

Importantly, we did not observe any further increase of immobilized CSB at longer time points after irradiation in XPA KO cells nor after spironolactone treatment, in contrast to the still increasing amount in CSA KO cells and in cells treated with CRL-activity inhibitor NAE1i. These observations suggest that part of the time-dependent dissociation is achieved by an active CSA-dependent process, which is most likely mediated by its ubiquitylation activity.

3.6. Development of fluorescence-based single-cell assay

Several labs, including our own (see also below), have conducted a variety of screens to identify factors associated with TC-NER [13,17,46–50]. These endeavors have created a wealth of potential TC-NER regulating factors, some of which have been characterized, though a large number await further validation. Our data illustrate that the generated fluorescently-tagged CSB KI cell line, in combination with FRAP-analysis to monitor chromatin binding of CSB, provides an unprecedented highly sensitive method to study TC-NER kinetics in living cells. Unfortunately, however, FRAP analysis is not particularly suited for high-throughput analyses to assess the significance for TC-NER of newly identified factors. Therefore, we developed a user-friendly, fluorescence-based single-cell assay in a 96-well format to measure TC-NER performance (see methods and Fig. 5A). This assay is evolved from our obtained knowledge on CSB's dynamic binding/dissociation to TBL-containing chromatin, in which we measure the DNA damage-induced nuclear retention of CSB-mClover after pre-extraction of non-bound molecules.

For this assay we first generated CSB-mClover KI in U2OS cells (CSB KI), as these adhere more effectively to 96-well plates than HCT116 cells. CSB KI and the corresponding KO cell lines were confirmed by immunoblot analysis, sequencing, and subsequently by FRAP assays (Supplementary Fig. 7A-D). The data corroborated and validated the results on CSB mobility in a different cell line, with even a greater dynamic window of immobilization. Chromatin-binding of CSB was determined using an automated reader for the 96-well plate format at 1 and 7 h after UV-irradiation in WT, CSA and UVSSA KO cell lines. Prolonged nuclear retention of CSB-mClover was evident in TC-NER deficient CSA KO cells. In contrast, loss of UVSSA triggered depletion of the CSB-mClover derived fluorescence, due to absence of recruitment of USP7 that protects CSB from degradation (Fig. 5B-C). This newly developed assay provides a highly reproducible, quantitative and sensitive readout to monitor UV-damage-induced TC-NER progression. Additionally, this assay can be extended to other DNA-damaging agents and the study of new candidate genes by knockdown (KD) or KO. This assay holds potential as a diagnostic tool for NER-related disorders and as a research tool for obtaining new insights into the mechanism and regulation of TC-NER.

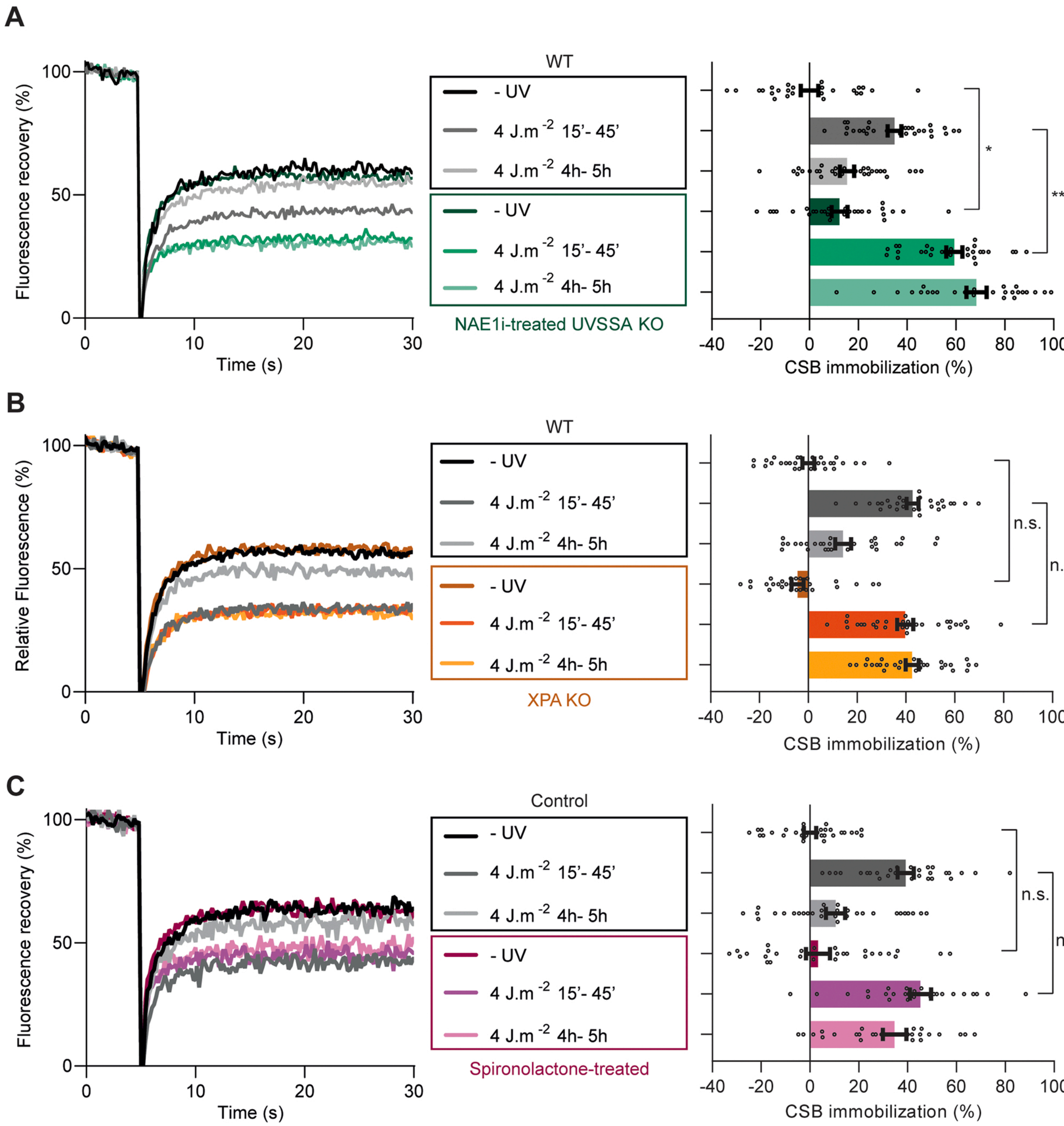

Fig. 4. UVSSA protects CSB from CRL-dependent degradation, and impaired TC-NER progression affects CSB release. (A-C) Left panels: FRAP analysis of CSB-mC KI cells. (A) WT KI (grey shades) and 10 μM NAE1i- treated UVSSA KO (turquoise shades). (B) Comparison of WT (grey shades) and XPA KO (orange shades). (C) WT cells mock (grey shades) and spironolactone-treated (lilac shades). Cells were mock or UV-C-irradiated (4 $J.m^{-2}$) and measured at the indicated time points. CSB-mClover fluorescence recovery was measured and normalized as described in Fig. 2. Right panels: Percentage of CSB-mClover immobile fraction in CSB-mC KI cells calculated from FRAP analysis shown in the left panel, as described in Fig. 2. Graphs and FRAP curves depict the mean ± S.E.M. of 30 cells from three independent experiments. * * $P < 0.01$, * ** $P < 0.001$, * ** * $P < 0.0001$, n.s. non-significant, analyzed by unpaired, two-tailed *t*- test (adjusted for multiple comparisons, see "Methods").

3.7. Interaction partners of CSB in deficient and proficient cells for TC-NER

Our live studies revealed different kinetic behavior of CSB-mClover in terms of chromatin binding in the absence of downstream TC-NER factors CSA (Fig. 3B), UVSSA (Fig. 4A), or XPA (Fig. 4B), respectively. This likely reflects divergent fates of TBL-stalled RNAPII when TC-NER progression is compromised at different stages. Transitions between different reaction steps were commonly regulated by transient protein-protein interactions and post-translational modifications, which are intrinsically difficult to capture by classical biochemical, cell fraction and live cell studies. Therefore, we further exploited our versatile CSB-mC KI cell line tool and its cognate CSA, UVSSA and XPA KO cell lines to identify interacting factors, including more transient interactors, that may be trapped by the absence of TC-NER progression. To that aim we used the mClover tag as bait to specifically purify CSB-mClover-interacting proteins through an established GFP-Trap [51] immuno-affinity pull down procedure, coupled to quantitative mass-spectrometry (MS) using Stable Isotope Labelling by

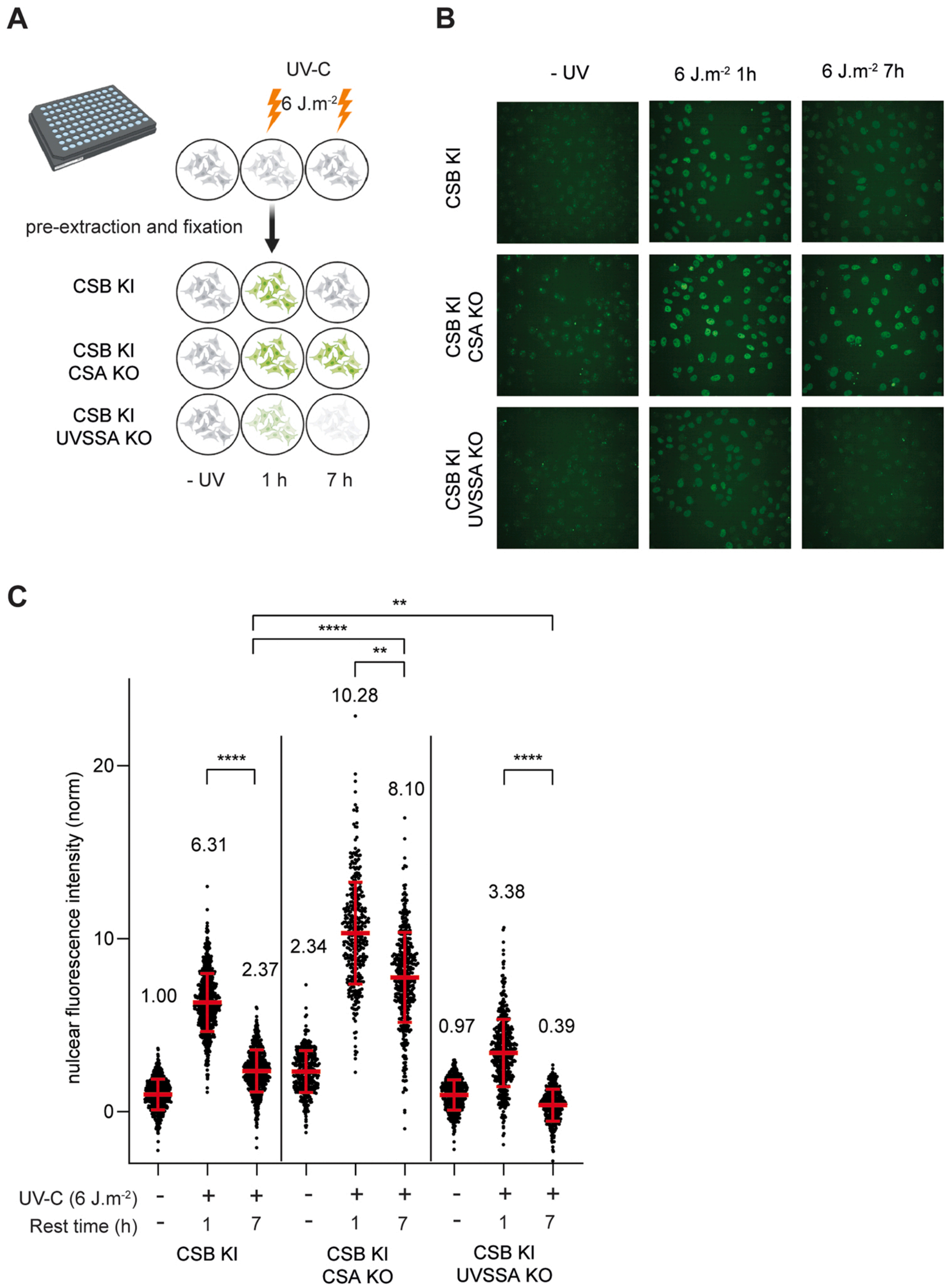

Fig. 5. Fluorescence-based single-cell assay. (A) Scheme depicting the workflow with expected retained nuclear fluorescence in the different genetic backgrounds. (B) Representative images and (C) quantification of endogenous CSB-mClover-derived fluorescence in U2OS CSB KI (WT, CSA or UVSSA KO), at the indicated time points after UV irradiation (6 J.m^{-2}). Data were normalized to nuclear background and to non-irradiated condition. Mean nuclear fluorescence intensities were provided in numbers above each condition ± S.D. of, respectively, n = 2771, 2449, 1889, 984, 793, 945, 1701, 1000, 1199 cells from 3 independent experiments. $**P < 0.01$, $***P < 0.001$, $****P < 0.0001$, n.s. non-significant, analyzed by a nested one-way ANOVA (adjusted for multiple comparison, see “Methods”).

Amino acids in Cell culture (SILAC) [39] to compare the persistent presence of non-functional protein complexes at TBLs in knock-out to proficient TC-NER cells. The experiment was conducted in duplicate with a label swap (see Fig. 6A and Methods for SILAC labeling). CSB has been found to reside in different protein complexes and cellular compartments with other suggested cellular functions not related to TC-NER [52], which may mask the TC-NER dedicated function. For that reason, cellular fractionation was applied to limit the assessment of the formation and activation of the multi-protein complex to the chromatin context in which TC-NER is acting. CSB-complexes were immunoprecipitated (GFP-Trap) from the chromatin fraction of cell lysates 30 min after 30 J.m^{-2} UV-C irradiation, since CSB is strongly bound to chromatin without significant degradation (even in UVSSA KO cells) at this time point (Fig. 1C, Supplementary Fig. 4D,5F,6A).

MS analysis identified several known CSB-specific interacting proteins in WT cells, including CRL4^{CSA}, UVSSA, RNAPII, TFIIH, the PAF-complex, DCLRE1A and other previously found interacting proteins [46,50,53], validating our approach (Fig. 6B and Table S1). Excitingly, several interesting interactions emerged as strongly bound to CSB in the different KO cells (Fig. 6C-E; Table S1). Since this manuscript is not about dissecting the TC-NER proteome, but is merely illustrating the far-reaching versatility of our developed tool for live cell imaging, only a few of them will be shortly discussed. In CSA KO, multiple proteins were detected to stably bind CSB upon DNA damage (Fig. 6C; Table S1). Among them several factors, previously described to act in other DDR processes: MCM9 DNA helicase (MCM9), which is involved in the removal of double strand breaks and is important for DNA mismatch repair [54,55]; PSMB4 and ATP2C1, which are both linked to DDR [56]. Interestingly, ACTN1, ACTN4, PPP1R18, MYO6, DBN1, CRACD, SATB2, SSFA2, ZMYM3 were also strongly recruited. These proteins are related to nuclear actin filaments and proposed to contribute to the chromatin structure which may be affected after DNA damage induction and

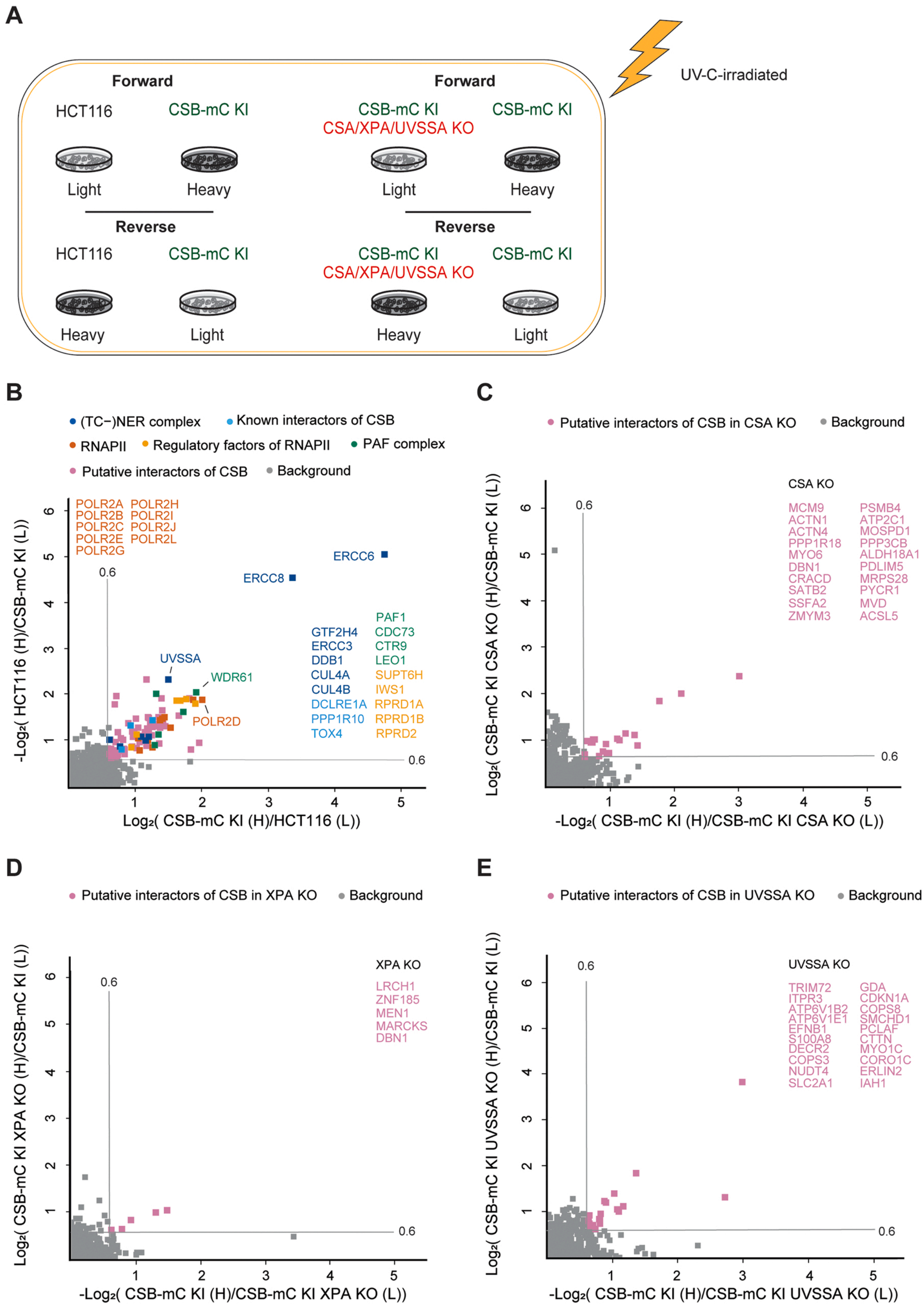

Fig. 6. Quantitative CSB-mClover interaction proteomics. (A) Schematic representation of the SILAC experiments including the label swap (Forward/Reverse). (B-E) Interaction proteomics in CSB-mC KI cells (B) WT; (C) CSA KO; (D) XPA KO; and (E) UVSSA KO. Scatter plot of $\log_2$ SILAC ratios of proteins isolated by GFP-pulldown, conducted in duplicate with a label swap. Cells were UV-C irradiated with 30 $J.m^{-2}$ and collected 30 min after irradiation. The (-) $\log_2$ SILAC ratios of proteins identified in the forward experiment (*x*-axis) are plotted against the (-) $\log_2$ SILAC ratios of proteins identified in the reversed experiment (*y*-axis), as indicated on the axes. Proteins were classified as specific CSB interactors (marked in color and assigned to a category according to the color legend) when $\log_2$ (SILAC ratio) > 0.6 (indicated by gray line) in both replicates.

arrested TC-NER.

We note that also in XPA KO actin related proteins MARCKS, DBN1 and ZNF185 showed strong interactions with CSB (Fig. 6D; Table S1). ZNF185 was recently described as p53 target after DNA damage [57]. Furthermore, MEN1 was markedly recruited to CSB after UV irradiation as well. MEN1 is a component of a histone methyltransferase complex, which interacts with FANCD2 [58].

Similarly, we examined the changes in the CSB interactome upon UV irradiation in UVSSAKO cells and surprisingly, the predominant CSB-specific interacting proteins were lost (Table S1). For example, interactions with RNAPII, TFIIH and PAF complex, along with several partners of CSB upon UV-irradiation were markedly reduced, supporting the idea that UVSSA is important to stabilize the TC-NER complex at TBLs. Similar to the CSA and XPA KO cells, we also detected CTTN, MYOC1 and CORO1C factors, which are required for actin rearrangement and contribute to the DDR [59,60]. Surprisingly, PCLAF was strongly recruited in UVSSA KO, which is related to DNA damage bypass and UV-C sensitivity [61,62].

Although further mechanistic studies will be required, the identification of these CSB-associated proteins under different conditions, illustrate the utility of the fluorescent protein (here mClover) tag inserted at, and expressed from, the endogenous gene locus of interest. An additional advantage of using the same tag for imaging and protein-association studies, is that the effect of newly identified TC-NER interactors can be directly monitored in live cell imaging mode in the same cell line through e.g., depletion, knockdown or knockout of the newly identified factor.

4. Concluding remarks

Previous knock-in strategies to study live cell DNA repair dynamics of endogenously expressed fluorescently-tagged DNA repair proteins were built on laborious gene targeting and tedious selection procedures in mouse embryonic stem cells. These studies have provided important novel information on repair protein dynamics and DDR kinetics [63] and cell-type specific repair activity and protein concentrations [28,64]. With the advent of CRSIPR/Cas9-mediated genome editing, live cell DDR imaging has entered a new era by allowing a more straight-forward generation of knock-in fluorescently tagged proteins expressed from their endogenous gene locus in different somatic cells and model animals [27,30–34,65–67].

Here we discuss the generation and application of endogenously tagged CSB, with the fluorescent protein (mClover), knock-in cell line. We showed that this cell line represents a unique and powerful tool with unprecedented sensitivity to monitor the action of the TC-NER process in living cells using relative very low doses of UV and thus provides an important advance in dissecting this process in different cellular systems.

The persistent stalling of RNAPII at TBLs triggers a strong DNA damage response, which coordinates several cellular processes by post-translational protein modifications, including the dynamic ubiquitylation [8,18]. Recently, ubiquitylation of RNAPII was identified as a crucial step in the TC-NER process, in which CSB, CSA and UVSSA were crucial to coordinate the ubiquitylation dynamics that drive this repair mechanism [8]. Despite the knowledge that CSB and CSA are associated with RNAPII at TBLs and that the CSA recruitment is completely dependent on CSB [17,68], a major unresolved question is whether the ubiquitin ligase activity of CRL4^{CSA} could modulate functional characteristics of CSB. Strikingly, we found that the immobile fraction of CSB was markedly increased at 4 h after UV irradiation in cells treated with NAE1i and in CSA KO cells, to a larger extent than in XPA KO cells, suggesting that the CRL4^{CSA} activity orchestrates the CSB binding at UV-induced DNA damage.

CSB was identified as one of the CRL4^{CSA} targets of UV-induced ubiquitylation and the subsequent degradation by the ubiquitin-proteasome pathway [9]. We also found a strong UV-induced CSB degradation in the absence of UVSSA, but only marginally in TC-NER-proficient cells. These data are in line with the proposed role of UVSSA in recruiting the USP7 deubiquitylase to counteract CSB ubiquitylation and its consequent degradation [13,15]. Together these data suggest that CSA-dependent release of CSB from TBL-stalled RNAPII as we observe here is mainly derived from other ubiquitin-mediated processes that drive TC-NER progression rather than from CRL4^{CSA}-induced proteasomal degradation of CSB.

Here we summarize the versatile applications of CSB-mClover KI cells, which are a highly sensitive tool to monitor TC-NER kinetics in living cells. In addition, we showed that these mClover KI cell lines were also valuable to investigate the composition of the TC-NER complex by mass spectrometry using affinity purification. The proteomic approach provided a comprehensive view of the protein network triggered by UV irradiation in knockout cell lines for TC-NER factors. Intriguing connections to nuclear architecture and genome organization, involving actin and its associated proteins were prominent identified in knockout cells. These proteins participate in a continuously expanding list of core processes within eukaryotic nuclei, including the maintenance of genomic integrity [69]. In response to DNA damage, nuclear actin and associated proteins are involved in the repair of damaged DNA through incompletely defined mechanisms. Future experiments are required to reveal the significance of these nuclear structural elements in the DDR.

CRediT authorship contribution statement

Diana A. Llerena Schiffmacher: conceptualization, data curation, formal analysis, investigation, methodology, supervision, validation, visualization, writing – original draft, writing – review & editing, ***Katarzyna W. Kliza***: conceptualization, investigation, data curation, methodology, writing – review & editing, ***Arjan F. Theil:*** conceptualization, investigation, methodology, writing – review & editing, ***Gert-Jan Kremers***: data curation, formal analysis, methodology, writing – review & editing, ***Jeroen A.A. Demmers:*** data curation, formal analysis, methodology, resources, validation, writing – review & editing, ***Tomoo Ogi:*** methodology, resources, writing – review & editing***, Michiel Vermeulen***: conceptualization, resources, methodology, writing – review & editing, ***Wim Vermeulen:*** conceptualization, funding acquisition, project administration, resources, supervision, writing – original draft, writing – review & editing, ***Alex Pines:*** conceptualization, data curation, formal analysis, investigation, project administration, resources, supervision, writing – original draft, writing – review & editing.

Declaration of Competing Interest

The authors declare that they have no known competing financial interests or personal relationships that could have appeared to influence the work reported in this paper.

Data Availability

Data will be made available on request.

Acknowledgement

This work was supported by the CW-TOP grant (714.017.003) and Oncode Institute (partly financed by the Dutch Cancer Society). We thank the Josephine Nefkens Cancer Program for infrastructural support. We thank Dr. Hannes Lans and Prof dr. Jurgen Marteijn for the constructive discussion.

Appendix A. Supporting information

Supplementary data associated with this article can be found in the online version at doi:10.1016/j.dnarep.2023.103566.

References

[1] J.H. Hoeijmakers, DNA damage, aging, and cancer, N. Engl. J. Med. 361 (2009) 1475–1485, https://doi.org/10.1056/NEJMra0804615.
[2] J.A. Marteijn, H. Lans, W. Vermeulen, J.H. Hoeijmakers, Understanding nucleotide excision repair and its roles in cancer and ageing, Nat. Rev. Mol. Cell Biol. 15 (2014) 465–481, https://doi.org/10.1038/nrm3822.
[3] J. Xu, I. Lahiri, W. Wang, A. Wier, M.A. Cianfrocco, J. Chong, A.A. Hare, P. B. Dervan, F. DiMaio, A.E. Leschziner, D. Wang, Structural basis for the initiation of eukaryotic transcription-coupled DNA repair, Nature 551 (2017) 653–657, https://doi.org/10.1038/nature24658.
[4] C. Troelstra, A. van Gool, J. de Wit, W. Vermeulen, D. Bootsma, J.H. Hoeijmakers, ERCC6, a member of a subfamily of putative helicases, is involved in Cockayne's syndrome and preferential repair of active genes, Cell 71 (1992) 939–953, https://doi.org/10.1016/0092-8674(92)90390-x.
[5] V. van den Boom, E. Citterio, D. Hoogstraten, A. Zotter, J.M. Egly, W.A. van Cappellen, J.H. Hoeijmakers, A.B. Houtsmuller, W. Vermeulen, DNA damage stabilizes interaction of CSB with the transcription elongation machinery, J. Cell Biol. 166 (2004) 27–36, https://doi.org/10.1083/jcb.200401056.
[6] C.P. Selby, A. Sancar, Cockayne syndrome group B protein enhances elongation by RNA polymerase II, Proc. Natl. Acad. Sci. U. S. A. 94 (1997) 11205–11209, https://doi.org/10.1073/pnas.94.21.11205.
[7] E.S. Fischer, A. Scrima, K. Bohm, S. Matsumoto, G.M. Lingaraju, M. Faty, T. Yasuda, S. Cavadini, M. Wakasugi, F. Hanaoka, S. Iwai, H. Gut, K. Sugasawa, N. H. Thoma, The molecular basis of CRL4DDB2/CSA ubiquitin ligase architecture, targeting, and activation, Cell 147 (2011) 1024–1039, https://doi.org/10.1016/j.cell.2011.10.035.
[8] Y. Nakazawa, Y. Hara, Y. Oka, O. Komine, D. van den Heuvel, C. Guo, Y. Daigaku, M. Isono, Y. He, M. Shimada, K. Kato, N. Jia, S. Hashimoto, Y. Kotani, Y. Miyoshi, M. Tanaka, A. Sobue, N. Mitsutake, T. Suganami, A. Masuda, K. Ohno, S. Nakada, T. Mashimo, K. Yamanaka, M.S. Luijsterburg, T. Ogi, Ubiquitination of DNA damage-stalled RNAPII promotes transcription-coupled repair, e1224, Cell 180 (2020) 1228–1244, https://doi.org/10.1016/j.cell.2020.02.010.
[9] R. Groisman, I. Kuraoka, O. Chevallier, N. Gaye, T. Magnaldo, K. Tanaka, A. F. Kisselev, A. Harel-Bellan, Y. Nakatani, CSA-dependent degradation of CSB by the ubiquitin-proteasome pathway establishes a link between complementation factors of the Cockayne syndrome, Genes Dev. 20 (2006) 1429–1434, https://doi.org/10.1101/gad.378206.
[10] G. Kokic, F.R. Wagner, A. Chernev, H. Urlaub, P. Cramer, Structural basis of human transcription-DNA repair coupling, Nature 598 (2021) 368–372, https://doi.org/10.1038/s41586-021-03906-4.
[11] D.M. Duda, L.A. Borg, D.C. Scott, H.W. Hunt, M. Hammel, B.A. Schulman, Structural insights into NEDD8 activation of cullin-RING ligases: conformational control of conjugation, Cell 134 (2008) 995–1006, https://doi.org/10.1016/j.cell.2008.07.022.
[12] R. Groisman, J. Polanowska, I. Kuraoka, J. Sawada, M. Saijo, R. Drapkin, A. F. Kisselev, K. Tanaka, Y. Nakatani, The ubiquitin ligase activity in the DDB2 and CSA complexes is differentially regulated by the COP9 signalosome in response to DNA damage, Cell 113 (2003) 357–367, https://doi.org/10.1016/s0092-8674(03)00316-7.
[13] P. Schwertman, A. Lagarou, D.H. Dekkers, A. Raams, A.C. van der Hoek, C. Laffeber, J.H. Hoeijmakers, J.A. Demmers, M. Fousteri, W. Vermeulen, J. A. Marteijn, UV-sensitive syndrome protein UVSSA recruits USP7 to regulate transcription-coupled repair, Nat. Genet 44 (2012) 598–602, https://doi.org/10.1038/ng.2230.
[14] Y. Nakazawa, K. Sasaki, N. Mitsutake, M. Matsuse, M. Shimada, T. Nardo, Y. Takahashi, K. Ohyama, K. Ito, H. Mishima, M. Nomura, A. Kinoshita, S. Ono, K. Takenaka, R. Masuyama, T. Kudo, H. Slor, A. Utani, S. Tateishi, S. Yamashita, M. Stefanini, A.R. Lehmann, K. Yoshiura, T. Ogi, Mutations in UVSSA cause UV-sensitive syndrome and impair RNA polymerase IIo processing in transcription-coupled nucleotide-excision repair, Nat. Genet. 44 (2012) 586–592, https://doi.org/10.1038/ng.2229.
[15] X. Zhang, K. Horibata, M. Saijo, C. Ishigami, A. Ukai, S. Kanno, H. Tahara, E. G. Neilan, M. Honma, T. Nohmi, A. Yasui, K. Tanaka, Mutations in UVSSA cause UV-sensitive syndrome and destabilize ERCC6 in transcription-coupled DNA repair, Nat. Genet. 44 (2012) 593–597, https://doi.org/10.1038/ng.2228.
[16] M. Okuda, Y. Nakazawa, C. Guo, T. Ogi, Y. Nishimura, Common TFIIH recruitment mechanism in global genome and transcription-coupled repair subpathways, Nucleic Acids Res. 45 (2017) 13043–13055, https://doi.org/10.1093/nar/gkx970.
[17] Y. van der Weegen, H. Golan-Berman, T.E.T. Mevissen, K. Apelt, R. Gonzalez-Prieto, J. Goedhart, E.E. Heilbrun, A.C.O. Vertegaal, D. van den Heuvel, J. C. Walter, S. Adar, M.S. Luijsterburg, The cooperative action of CSB, CSA, and UVSSA target TFIIH to DNA damage-stalled RNA polymerase II, Nat. Commun. 11 (2020) 2104, https://doi.org/10.1038/s41467-020-15903-8.
[18] A. Tufegdzic Vidakovic, R. Mitter, G.P. Kelly, M. Neumann, M. Harreman, M. Rodriguez-Martinez, A. Herlihy, J.C. Weems, S. Boeing, V. Encheva, L. Gaul, L. Milligan, D. Tollervey, R.C. Conaway, J.W. Conaway, A.P. Snijders, A. Stewart, J.Q. Svejstrup, Regulation of the RNAPII pool is integral to the DNA damage response, e1221, Cell 180 (2020) 1245–1261, https://doi.org/10.1016/j.cell.2020.02.009.
[19] M. Chalfie, Y. Tu, G. Euskirchen, W.W. Ward, D.C. Prasher, Green fluorescent protein as a marker for gene expression, Science 263 (1994) 802–805, https://doi.org/10.1126/science.8303295.
[20] W. Vermeulen, Dynamics of mammalian NER proteins, DNA Repair (Amst.) 10 (2011) 760–771, https://doi.org/10.1016/j.dnarep.2011.04.015.
[21] A.B. Houtsmuller, W. Vermeulen, Macromolecular dynamics in living cell nuclei revealed by fluorescence redistribution after photobleaching, Histochem Cell Biol. 115 (2001) 13–21, https://doi.org/10.1007/s004180000234.
[22] C. Dinant, M. de Jager, J. Essers, W.A. van Cappellen, R. Kanaar, A.B. Houtsmuller, W. Vermeulen, Activation of multiple DNA repair pathways by sub-nuclear damage induction methods, J. Cell Sci. 120 (2007) 2731–2740, https://doi.org/10.1242/jcs.004523.
[23] A.B. Houtsmuller, S. Rademakers, A.L. Nigg, D. Hoogstraten, J.H. Hoeijmakers, W. Vermeulen, Action of DNA repair endonuclease ERCC1/XPF in living cells, Science 284 (1999) 958–961, https://doi.org/10.1126/science.284.5416.958.
[24] S. Rademakers, M. Volker, D. Hoogstraten, A.L. Nigg, M.J. Mone, A.A. Van Zeeland, J.H. Hoeijmakers, A.B. Houtsmuller, W. Vermeulen, Xeroderma pigmentosum group A protein loads as a separate factor onto DNA lesions, Mol. Cell Biol. 23 (2003) 5755–5767, https://doi.org/10.1128/MCB.23.16.5755-5767.2003.
[25] D. Hoogstraten, A.L. Nigg, H. Heath, L.H. Mullenders, R. van Driel, J. H. Hoeijmakers, W. Vermeulen, A.B. Houtsmuller, Rapid switching of TFIIH between RNA polymerase I and II transcription and DNA repair in vivo, Mol. Cell 10 (2002) 1163–1174, https://doi.org/10.1016/s1097-2765(02)00709-8.
[26] L. van Cuijk, G.J. van Belle, Y. Turkyilmaz, S.L. Poulsen, R.C. Janssens, A.F. Theil, M. Sabatella, H. Lans, N. Mailand, A.B. Houtsmuller, W. Vermeulen, J.A. Marteijn, SUMO and ubiquitin-dependent XPC exchange drives nucleotide excision repair, Nat. Commun. 6 (2015) 7499, https://doi.org/10.1038/ncomms8499.
[27] C. Ribeiro-Silva, M. Sabatella, A. Helfricht, J.A. Marteijn, A.F. Theil, W. Vermeulen, H. Lans, Ubiquitin and TFIIH-stimulated DDB2 dissociation drives DNA damage handover in nucleotide excision repair, Nat. Commun. 11 (2020) 4868, https://doi.org/10.1038/s41467-020-18705-0.
[28] G. Giglia-Mari, A.F. Theil, P.O. Mari, S. Mourgues, J. Nonnekens, L.O. Andrieux, J. de Wit, C. Miquel, N. Wijgers, A. Maas, M. Fousteri, J.H. Hoeijmakers, W. Vermeulen, Differentiation driven changes in the dynamic organization of basal transcription initiation, PLoS Biol. 7 (2009), e1000220, https://doi.org/10.1371/journal.pbio.1000220.
[29] S.H. Sternberg, J.A. Doudna, Expanding the biologist's toolkit with CRISPR-Cas9, Mol. Cell 58 (2015) 568–574, https://doi.org/10.1016/j.molcel.2015.02.032.
[30] C. Carrasco-Padilla, P. Roda-Navarro, CRISPR/Cas9-mediated genome editing assists protein dynamics studies in live cells, Eur. J. Cell Biol. 101 (2022), 151203, https://doi.org/10.1016/j.ejcb.2022.151203.
[31] B. Koch, B. Nijmeijer, M. Kueblbeck, Y. Cai, N. Walther, J. Ellenberg, Generation and validation of homozygous fluorescent knock-in cells using CRISPR-Cas9 genome editing, Nat. Protoc. 13 (2018) 1465–1487, https://doi.org/10.1038/nprot.2018.042.
[32] H. Bukhari, T. Muller, Endogenous fluorescence tagging by CRISPR, Trends Cell Biol. 29 (2019) 912–928, https://doi.org/10.1016/j.tcb.2019.08.004.
[33] B. Steurer, R.C. Janssens, B. Geverts, M.E. Geijer, F. Wienholz, A.F. Theil, J. Chang, S. Dealy, J. Pothof, W.A. van Cappellen, A.B. Houtsmuller, J.A. Marteijn, Live-cell analysis of endogenous GFP-RPB1 uncovers rapid turnover of initiating and promoter-paused RNA Polymerase II, Proc. Natl. Acad. Sci. U. S. A. 115 (2018) E4368–E4376, https://doi.org/10.1073/pnas.1717920115.
[34] B. Steurer, R.C. Janssens, M.E. Geijer, F. Aprile-Garcia, B. Geverts, A.F. Theil, B. Hummel, M.E. van Royen, B. Evers, R. Bernards, A.B. Houtsmuller, R. Sawarkar, J. Marteijn, DNA damage-induced transcription stress triggers the genome-wide degradation of promoter-bound Pol II, Nat. Commun. 13 (2022) 3624, https://doi.org/10.1038/s41467-022-31329-w.
[35] J. Cox, N. Neuhauser, A. Michalski, R.A. Scheltema, J.V. Olsen, M. Mann, Andromeda: a peptide search engine integrated into the MaxQuant environment, J. Proteome Res. 10 (2011) 1794–1805, https://doi.org/10.1021/pr101065j.
[36] S. Tyanova, T. Temu, P. Sinitcyn, A. Carlson, M.Y. Hein, T. Geiger, M. Mann, J. Cox, The Perseus computational platform for comprehensive analysis of (prote)omics data, Nat. Methods 13 (2016) 731–740, https://doi.org/10.1038/nmeth.3901.
[37] T.D. Parks, K.K. Leuther, E.D. Howard, S.A. Johnston, W.G. Dougherty, Release of proteins and peptides from fusion proteins using a recombinant plant virus proteinase, Anal. Biochem. 216 (1994) 413–417, https://doi.org/10.1006/abio.1994.1060.
[38] B.T. Bajar, E.S. Wang, A.J. Lam, B.B. Kim, C.L. Jacobs, E.S. Howe, M.W. Davidson, M.Z. Lin, J. Chu, Improving brightness and photostability of green and red fluorescent proteins for live cell imaging and FRET reporting, Sci. Rep. 6 (2016) 20889, https://doi.org/10.1038/srep20889.
[39] A.H. Smits, M. Vermeulen, Characterizing protein-protein interactions using mass spectrometry: challenges and opportunities, Trends Biotechnol. 34 (2016) 825–834, https://doi.org/10.1016/j.tibtech.2016.02.014.
[40] R.J. Lake, A. Geyko, G. Hemashettar, Y. Zhao, H.Y. Fan, UV-induced association of the CSB remodeling protein with chromatin requires ATP-dependent relief of N-terminal autorepression, Mol. Cell 37 (2010) 235–246, https://doi.org/10.1016/j.molcel.2009.10.027.
[41] F. Liebelt, J. Schimmel, M. Verlaan-de Vries, E. Klemann, M.E. van Royen, Y. van der Weegen, M.S. Luijsterburg, L.H. Mullenders, A. Pines, W. Vermeulen, A.C. O. Vertegaal, Transcription-coupled nucleotide excision repair is coordinated by ubiquitin and SUMO in response to ultraviolet irradiation, Nucleic Acids Res. 48 (2020) 231–248, https://doi.org/10.1093/nar/gkz977.
[42] T.A. Soucy, P.G. Smith, M.A. Milhollen, A.J. Berger, J.M. Gavin, S. Adhikari, J. E. Brownell, K.E. Burke, D.P. Cardin, S. Critchley, C.A. Cullis, A. Doucette, J. J. Garnsey, J.L. Gaulin, R.E. Gershman, A.R. Lublinsky, A. McDonald, H. Mizutani, U. Narayanan, E.J. Olhava, S. Peluso, M. Rezaei, M.D. Sintchak, T. Talreja, M. P. Thomas, T. Traore, S. Vyskocil, G.S. Weatherhead, J. Yu, J. Zhang, L.R. Dick, C. F. Claiborne, M. Rolfe, J.B. Bolen, S.P. Langston, An inhibitor of NEDD8-activating

enzyme as a new approach to treat cancer, Nature 458 (2009) 732–736, https://doi.org/10.1038/nature07884.
[43] C.L. Li, F.M. Golebiowski, Y. Onishi, N.L. Samara, K. Sugasawa, W. Yang, Tripartite DNA lesion recognition and verification by XPC, TFIIH, and XPA in nucleotide excision repair, Mol. Cell 59 (2015) 1025–1034, https://doi.org/10.1016/j.molcel.2015.08.012.
[44] A.K. Chauhan, P. Li, Y. Sun, G. Wani, Q. Zhu, A.A. Wani, Spironolactone-induced XPB degradation requires TFIIH integrity and ubiquitin-selective segregase VCP/p97, Cell Cycle 20 (2021) 81–95, https://doi.org/10.1080/15384101.2020.1860559.
[45] S. Alekseev, M. Ayadi, L. Brino, J.M. Egly, A.K. Larsen, F. Coin, A small molecule screen identifies an inhibitor of DNA repair inducing the degradation of TFIIH and the chemosensitization of tumor cells to platinum, Chem. Biol. 21 (2014) 398–407, https://doi.org/10.1016/j.chembiol.2013.12.014.
[46] S. Boeing, L. Williamson, V. Encheva, I. Gori, R.E. Saunders, R. Instrell, O. Aygun, M. Rodriguez-Martinez, J.C. Weems, G.P. Kelly, J.W. Conaway, R.C. Conaway, A. Stewart, M. Howell, A.P. Snijders, J.Q. Svejstrup, Multiomic analysis of the UV-induced DNA damage response, Cell Rep. 15 (2016) 1597–1610, https://doi.org/10.1016/j.celrep.2016.04.047.
[47] F. Wienholz, D. Zhou, Y. Turkyilmaz, P. Schwertman, M. Tresini, A. Pines, M. van Toorn, K. Bezstarosti, J.A.A. Demmers, J.A. Marteijn, FACT subunit Spt16 controls UVSSA recruitment to lesion-stalled RNA Pol II and stimulates TC-NER, Nucleic Acids Res. 47 (2019) 4011–4025, https://doi.org/10.1093/nar/gkz055.
[48] M. Olivieri, T. Cho, A. Alvarez-Quilon, K. Li, M.J. Schellenberg, M. Zimmermann, N. Hustedt, S.E. Rossi, S. Adam, H. Melo, A.M. Heijink, G. Sastre-Moreno, N. Moatti, R.K. Szilard, A. McEwan, A.K. Ling, A. Serrano-Benitez, T. Ubhi, S. Feng, J. Pawling, I. Delgado-Sainz, M.W. Ferguson, J.W. Dennis, G.W. Brown, F. Cortes-Ledesma, R.S. Williams, A. Martin, D. Xu, D. Durocher, A genetic map of the response to DNA damage in human cells, e421, Cell 182 (2020) 481–496, https://doi.org/10.1016/j.cell.2020.05.040.
[49] M.E. Geijer, D. Zhou, K. Selvam, B. Steurer, C. Mukherjee, B. Evers, S. Cugusi, M. van Toorn, M. van der Woude, R.C. Janssens, Y.P. Kok, W. Gong, A. Raams, C.S. Y. Lo, J.H.G. Lebbink, B. Geverts, D.A. Plummer, K. Bezstarosti, A.F. Theil, R. Mitter, A.B. Houtsmuller, W. Vermeulen, J.A.A. Demmers, S. Li, M. van Vugt, H. Lans, R. Bernards, J.Q. Svejstrup, A. Ray Chaudhuri, J.J. Wyrick, J.A. Marteijn, Elongation factor ELOF1 drives transcription-coupled repair and prevents genome instability, Nat. Cell Biol. 23 (2021) 608–619, https://doi.org/10.1038/s41556-021-00692-z.
[50] D. van den Heuvel, C.G. Spruijt, R. Gonzalez-Prieto, A. Kragten, M.T. Paulsen, D. Zhou, H. Wu, K. Apelt, Y. van der Weegen, K. Yang, M. Dijk, L. Daxinger, J. A. Marteijn, A.C.O. Vertegaal, M. Ljungman, M. Vermeulen, M.S. Luijsterburg, A CSB-PAF1C axis restores processive transcription elongation after DNA damage repair, Nat. Commun. 12 (2021) 1342, https://doi.org/10.1038/s41467-021-21520-w.
[51] P.C. Fridy, Y. Li, S. Keegan, M.K. Thompson, I. Nudelman, J.F. Scheid, M. Oeffinger, M.C. Nussenzweig, D. Fenyo, B.T. Chait, M.P. Rout, A robust pipeline for rapid production of versatile nanobody repertoires, Nat. Methods 11 (2014) 1253–1260, https://doi.org/10.1038/nmeth.3170.
[52] V. Tiwari, B.A. Baptiste, M.N. Okur, V.A. Bohr, Current and emerging roles of Cockayne syndrome group B (CSB) protein, Nucleic Acids Res 49 (2021) 2418–2434, https://doi.org/10.1093/nar/gkab085.
[53] T. Iyama, S.Y. Lee, B.R. Berquist, O. Gileadi, V.A. Bohr, M.M. Seidman, P. J. McHugh, D.M. Wilson 3rd, CSB interacts with SNM1A and promotes DNA interstrand crosslink processing, Nucleic Acids Res. 43 (2015) 247–258, https://doi.org/10.1093/nar/gku1279.
[54] K. Nishimura, M. Ishiai, K. Horikawa, T. Fukagawa, M. Takata, H. Takisawa, M. T. Kanemaki, Mcm8 and Mcm9 form a complex that functions in homologous recombination repair induced by DNA interstrand crosslinks, Mol. Cell 47 (2012) 511–522, https://doi.org/10.1016/j.molcel.2012.05.047.
[55] S. Traver, P. Coulombe, I. Peiffer, J.R. Hutchins, M. Kitzmann, D. Latreille, M. Mechali, MCM9 is required for mammalian DNA mismatch repair, Mol. Cell 59 (2015) 831–839, https://doi.org/10.1016/j.molcel.2015.07.010.
[56] S. Cialfi, L. Le Pera, C. De Blasio, G. Mariano, R. Palermo, A. Zonfrilli, D. Uccelletti, C. Palleschi, G. Biolcati, L. Barbieri, I. Screpanti, C. Talora, The loss of ATP2C1 impairs the DNA damage response and induces altered skin homeostasis: consequences for epidermal biology in Hailey-Hailey disease, Sci. Rep. 6 (2016) 31567, https://doi.org/10.1038/srep31567.
[57] A. Smirnov, A. Cappello, A.M. Lena, L. Anemona, A. Mauriello, N. Di Daniele, M. Annicchiarico-Petruzzelli, G. Melino, E. Candi, ZNF185 is a p53 target gene following DNA damage, Aging (Albany NY) 10 (2018) 3308–3326, https://doi.org/10.18632/aging.101639.
[58] S. Jin, H. Mao, R.W. Schnepp, S.M. Sykes, A.C. Silva, A.D. D'Andrea, X. Hua, Menin associates with FANCD2, a protein involved in repair of DNA damage, Cancer Res. 63 (2003) 4204–4210.
[59] M. Kulashreshtha, I.S. Mehta, P. Kumar, B.J. Rao, Chromosome territory relocation during DNA repair requires nuclear myosin 1 recruitment to chromatin mediated by Upsilon-H2AX signaling, Nucleic Acids Res. 44 (2016) 8272–8291, https://doi.org/10.1093/nar/gkw573.
[60] T. Venit, K. Semesta, S. Farrukh, M. Endara-Coll, R. Havalda, P. Hozak, P. Percipalle, Nuclear myosin 1 activates p21 gene transcription in response to DNA damage through a chromatin-based mechanism, Commun. Biol. 3 (2020) 115, https://doi.org/10.1038/s42003-020-0836-1.
[61] L. Turchi, M. Fareh, E. Aberdam, S. Kitajima, F. Simpson, C. Wicking, D. Aberdam, T. Virolle, ATF3 and p15PAF are novel gatekeepers of genomic integrity upon UV stress, Cell Death Differ. 16 (2009) 728–737, https://doi.org/10.1038/cdd.2009.2.
[62] L.K. Povlsen, P. Beli, S.A. Wagner, S.L. Poulsen, K.B. Sylvestersen, J.W. Poulsen, M. L. Nielsen, S. Bekker-Jensen, N. Mailand, C. Choudhary, Systems-wide analysis of ubiquitylation dynamics reveals a key role for PAF15 ubiquitylation in DNA-damage bypass, Nat. Cell Biol. 14 (2012) 1089–1098, https://doi.org/10.1038/ncb2579.
[63] M. Reuter, A. Zelensky, I. Smal, E. Meijering, W.A. van Cappellen, H.M. de Gruiter, G.J. van Belle, M.E. van Royen, A.B. Houtsmuller, J. Essers, R. Kanaar, C. Wyman, BRCA2 diffuses as oligomeric clusters with RAD51 and changes mobility after DNA damage in live cells, J. Cell Biol. 207 (2014) 599–613, https://doi.org/10.1083/jcb.201405014.
[64] L.M. Donnio, C. Miquel, W. Vermeulen, G. Giglia-Mari, P.O. Mari, Cell-type specific concentration regulation of the basal transcription factor TFIIH in XPB(y/y) mice model, Cancer Cell Int. 19 (2019) 237, https://doi.org/10.1186/s12935-019-0945-4.
[65] K.L. Thijssen, M. van der Woude, C. Davo-Martinez, D.H.W. Dekkers, M. Sabatella, J.A.A. Demmers, W. Vermeulen, H. Lans, C. elegans TFIIH subunit GTF-2H5/TTDA is a non-essential transcription factor indispensable for DNA repair, Commun. Biol. 4 (2021) 1336, https://doi.org/10.1038/s42003-021-02875-8.
[66] M. Sabatella, K.L. Thijssen, C. Davo-Martinez, W. Vermeulen, H. Lans, Tissue-specific DNA repair activity of ERCC-1/XPF-1, Cell Rep. 34 (2021), 108608, https://doi.org/10.1016/j.celrep.2020.108608.
[67] M.W. Paul, A. Sidhu, Y. Liang, S.E. van Rossum-Fikkert, H. Odijk, A.N. Zelensky, R. Kanaar, C. Wyman, Role of BRCA2 DNA-binding and C-terminal domain in its mobility and conformation in DNA repair, Elife 10 (2021), https://doi.org/10.7554/eLife.67926.
[68] S. Kamiuchi, M. Saijo, E. Citterio, M. de Jager, J.H. Hoeijmakers, K. Tanaka, Translocation of cockayne syndrome group A protein to the nuclear matrix: possible relevance to transcription-coupled DNA repair, Proc. Natl. Acad. Sci. U. S. A. 99 (2002) 201–206, https://doi.org/10.1073/pnas.012473199.
[69] A.M. Cobb, S.A. De Silva, R. Hayward, K. Sek, S. Ulferts, R. Grosse, C.M. Shanahan, Filamentous nuclear actin regulation of PML NBs during the DNA damage response is deregulated by prelamin A, Cell Death Dis. 13 (2022) 1042, https://doi.org/10.1038/s41419-022-05491-4.